iScience

Article

Competing signaling pathways controls electrotaxis

Graphical abstract

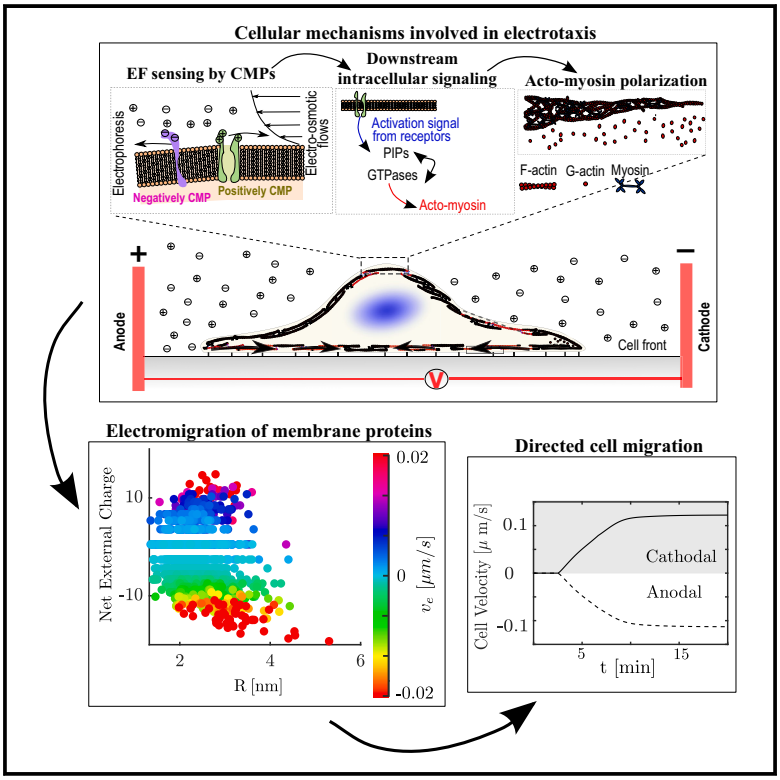

Highlights

- A mechanistic model that explains electrotaxis across different cell types
- Simultaneous polarization of membrane receptors sets cooperative and competing stimuli
- Using electric fields, directed cell migration is enhanced, canceled, or switched

Authors

S. Kulkarni, F. Tebar, C. Rentero, M. Zhao, P. Sáez

Correspondence

pablo.saez@upc.edu

In brief

Mechanobiology; Cell biology; Biophysics

Kulkarni et al., 2025, iScience *28*, 112329
May 16, 2025
https://doi.org/10.1016/j.isci.2025.112329

CellPress

iScience

CellPress
OPEN ACCESS

Article

Competing signaling pathways controls electrotaxis

S. Kulkarni,[1] F. Tebar,[2,3] C. Rentero,[2,3] M. Zhao,[4] and P. Sáez[1,5,6,*]

[1]Laboratori de Càlcul Numèric (LaCàN), ETS de Ingeniería de Caminos, Canales y Puertos, Universitat Politècnica de Catalunya, Barcelona, Spain

[2]Department of Biomedical Sciences, Faculty of Medicine and Health Sciences, University of Barcelona, 08036 Barcelona, Spain

[3]Cell Compartments and Signaling Group, Fundació de Recerca Clínic Barcelona - Institut d'Investigacions Biomèdiques August Pi i Sunyer (FRCB-IDIBAPS), 08036 Barcelona, Spain

[4]Department of Ophthalmology & Vision Science, School of Medicine, University of California, Davis, Sacramento, CA, USA

[5]IMTech (Institute of Mathematics), Universitat Politècnica de Catalunya-BarcelonaTech., 08034 Barcelona, Spain

[6]Lead contact

*Correspondence: pablo.saez@upc.edu

https://doi.org/10.1016/j.isci.2025.112329

SUMMARY

Understanding how cells follow exogenous cues is a key question for biology, medicine, and bioengineering. Growing evidence shows that electric fields represent a precise and programmable method to control cell migration. Most data suggest that the polarization of membrane proteins and the following downstream signaling are central to electrotaxis. Unfortunately, how these multiple mechanisms coordinate with the motile machinery of the cell is still poorly understood. Here, we develop a mechanistic model that explains electrotaxis across different cell types. Using the zebrafish proteome, we identify membrane proteins directly related to migration signaling pathways that polarize anodally and cathodally. Further, we show that the simultaneous and asymmetric distribution of these membrane receptors establish multiple cooperative and competing stimuli for directing the anodal and cathodal migration of the cell. Using electric fields, we enhance, cancel, or switch directed cell migration, with clear implications in promoting tissue regeneration or arresting tumor progression.

INTRODUCTION

Cell migration determines some of the most fundamental processes of life, such as embryonic development, wound healing, or tumor invasion, among many others.[1–3] Cells migrate guided by exogenous signals *in vivo* and *in vitro*. For decades, there have been tremendous efforts to understand how cells organize themselves and with others to follow stimuli in the form of chemical[4] and mechanical cues.[5,6] There is also an increasing interest in the life sciences and bioengineering in controlling cell migration through external cues because it may allow us to, e.g., arrest tumor cell invasion or promote tissue regeneration.[1,7,8] It may also allow us to precisely design the cellular structure in tissue constructs to achieve remarkable biomimetic features.[9,10]

Electrotaxis, the migration of cells under the influence of electric fields (EFs), represents a powerful and programmable form of guiding cell migration.[11–13] Numerous experimental observations are consistent with the hypothesis of electrotaxis. Indeed, electrotaxis is ubiquitous across different cell types, including cancer cells,[14] neurons[15] or leukocytes,[16] and tissues.[17,18] It also appears in different physiological conditions, e.g., during embryonic development[19] or wound healing.[20] Most studies have shown that cells migrate toward the cathode. However, we can also find cell types, or cells under specific conditions, that migrate toward the anode. Corneal epithelial cells (CECs) migrate to the cathode under the influence of an EF of 150 mV/mm in magnitude, which has been attributed to a cathodal distribution of epidermal growth factor receptor (EGFR) and membrane lipids.[21,22] This behavior was also found in mammalian epithelial cells (MECs) under the same EF strength,[23] with EGFR polarization and migration toward the cathode. Embryonic and adult neural progenitor cells show directed migration to the cathode in an EF of 500 mV/mm, which was reduced when PI3K/Akt was inhibited.[24] Human telomerase-immortalized corneal epithelial (hTCEpi) cells also undergo cathodal electrotaxis in the presence of an EF of 101.2 mV/mm,[25] as well as in fish keratocytes[26] and macrophages[27] in the presence of an EF of 400 mV/mm. Other studies showed that Chinese hamster ovary (CHO) cells migrate to the cathode or anode in an EF of 300 mV/mm depending on the presence of integrins.[28] EFs of around 75–100 mV/mm cause anodal migration of endothelial cells with an anodal polarization of vascular endothelial growth factor (VEGF) receptors, PI3K-Akt, and Rho signaling.[29] The same consistency in the migration and polarization of EGFR toward the anode was found in breast cancer cells.[30,31] Bone marrow mesenchymal stem cells and macrophages also show anodal migration.[27,32] Lung cancer cell lines CL1–5 (highly metastatic) and CL1–0 (weakly metastatic) have shown anodal and weak electrotaxis, respectively.[33] However, it was later demonstrated that CL1-5 cells accumulate EGFR and filopodia on the cathodal side[34] in an EGFR-independent migration mode.[35] On cell aggregates, glioblastoma and medulloblastoma migrate cathodally and

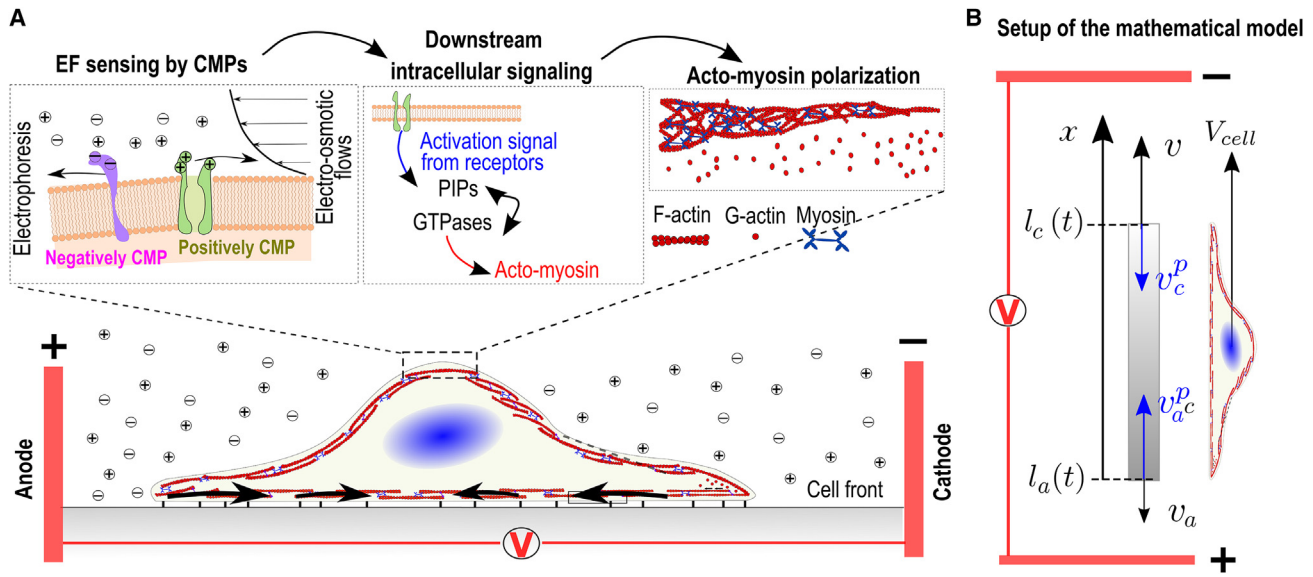

Figure 1. Mechanisms and model description

(A) Sketch of the main processes involved in electrotaxis. Left box: Two competing forces polarize charged cell membrane components. First, an EF exerts forces on the net electric charge of the cell membrane, pulling it in a certain direction (electrophoresis). The generation of an electroosmotic flow by the EF that transports soluble ions and fluid outside the cell (electroosmosis) also generates drag forces on the membrane proteins. Middle box: The polarization of membrane components induces intracellular signals involved in the cell polarization of the actomyosin network that controls the direction of migration (right box).

(B) A 1D electrotaxis model couples CMPs polarization, intracellular signals, and gel active models (see STAR Methods for details on the description of model variables and governing equations) to establish the cell migration velocity v (direction and magnitude). The retrograde flow, v^F, (black arrows) moves from the cathodal and anodal cell front inwards (sub-indexes c and a in the variables, respectively). The polymerization velocity (v_p, blue arrow) points outwards from the cell membrane. The position of the apical side of the cell is denoted by $l_a(t)$ and the one facing the cathodal one is denoted by $l_c(t)$.

anodally, respectively, in the same culture and stimulation conditions.[36]

Unfortunately, how cells follow the EF stimulus is not well understood and, therefore, important answers to the following questions remain elusive. For example, why do some cells migrate toward the anode while others migrate toward the cathode? What are the cell sensors that trigger electrotaxis? Are there universal mechanisms that explain electrotaxis across cell types? To answer these questions, we must understand three fundamental layers in the electrotaxis process: First, how an EF is sensed by the cell; second, how that signal is transferred intracellularly to finally control the migration machinery of the cell. We show a schematic representation of the main mechanisms involved in electrotaxis in Figure 1.

When an EF is applied to a cell, only cell components with an extracellular domain can sense it because the EF cannot enter the electrically insulated cytoplasm.[37] Therefore, cell membrane proteins are likely candidates for sensing an externally applied EF. Among several hypotheses, theoretical and experimental evidence has shown that electrotaxis is consistent with the electromotility model,[23,38,39] where the electromotility of charged membrane proteins (CMPs) with extracellular domains polarizes under the effect of an EF using electrophoresis and electroosmotic forces (see[38,40] and references therein). VEGF/EGF receptors,[23] integrins,[28] receptor tyrosine kinases (RTKs),[41] and G protein-coupled receptors (GPCRs) have been shown to polarize under EFs. Many of these proteins then trigger cell polarization through putative downstream signaling adaptation processes.[42–44] Some of these CMPs can also cluster in lipid rafts, creating complex compounds of molecules that also electro-migrate under an EF.[23,45]

Mechanistically, an EF, as any other tactic cue, must eventually control the physical forces that dictate cell migration. Cells migrate because of asymmetric intracellular forces that direct cells in specific directions. The forces involved in cell migration can be reduced to three: First, forces that protrude the cell membrane forward due to a continuous polymerization of actin filaments.[46–48] The extension of actin filaments, particularly at their fast-growing "barbed ends," is tightly regulated by various factors involved in nucleation, capping, and depolymerization of actin filaments.[49,50] Second, contractile forces generated by myosin motors induce an inward retrograde flow in the actomyosin network.[51–53] Third, adhesion forces that are transmitted from the internal actomyosin network to the extracellular space through molecules in the adhesion complexes.[54,55] Stronger adhesions mean higher effective friction in the retrograde flow which, consequently, slows it down while weak adhesions allow for faster retrograde flows.[56–58] The polarization and balance of these three forces ultimately determine the strength and direction of cell migration.

In connecting the initial polarization of CMPs in response to exogenous EFs and the final polarization of any of those three motile forces, there are intermediate signaling layers. Specifically, small GTPases of the rho family, phosphoinositide kinases, and phosphoinositides phosphate (PIPs) have fundamental roles

Table 1. Table of all abbreviations

Abbreviation	Definition
EF	Electric Field
CMP	Charged Membrane Proteins
EDL	Electrical Double Layer
EOF	Electro Osmotic Flow
CEC	Corneal Epithelial Cells
MEC	Mammalian Epithelial Cells
hTCEpi	Human Telomerase-immortalized Corneal Epithelial
CHO	Chinese Hamster Ovary
EGFR	Epidermal Growth Factor Receptor
VEGF	Vascular Endothelial Growth Factor
RTKs	Receptor Tyrosine Kinases
GTPases	Guanosine Triphosphates
PIPs	Phosphoinositides Phosphate
PI3K	Phosphoinositide 3-kinase
GPI	Glycosyl Phosphatidyl Inositol
GEFs	Guanine Nucleotide Exchange factors
GDP	Guanosine Diphosphate
GAPs	GTPase Activating Proteins
PTEN	Phosphatase and tensin homolog
LEGI	Local Excitation Global Inhibition

in cell polarization and migration.[59,60] Intricate feedback loops between Rho-GTPases, PIPs, phosphoinositides, and their activating stimuli determine what will become the front and back of the cell and, eventually, the cell migration direction. Understanding the coordination of these pathways in space and time is a fundamental goal for studying electrotaxis and cell migration in general. Further details and modeling options will be described in the following sections.

In short, there is direct experimental evidence of electrotaxis across multiple cell types. However, what specific sensors at the cell membrane trigger electrotaxis, how these CMPs first redistribute, and how they polarize the downstream signals that control the motility forces of the cell to, eventually, establish either an anodal or cathodal migration remains poorly understood. Here, we explore a mechanistic computational model to answer these questions by integrating models of electromigration of CMPs, signaling pathways, and cell migration which, as far as we know, has never been described before. This approach provides a complete, efficient, and adaptable way of analyzing all the elements that cooperate toward electrotaxis. To make this tool available for guiding future experimental research and further modeling efforts, we present the computational model in an online platform uploaded in the MATLAB Central File Exchange. We have also included Table 1 all the abbreviations used in the text for clarity.

RESULTS

Polarization of CMPs and intracellular signals explain electrotaxis

To analyze electrotaxis, we developed a one-dimensional computational model of electrotaxis. To make the reading of the article clearer, we summarize all model variables in Table 2 (see Section for further details of the model). In short, the first layer of the model corresponds to the polarization of CMPs, $\rho_{\pm}$, which represent the sensing components of the cell. The CMPs polarize due to EOF and electrophoretic forces, which effectively induce an electromigration velocity, v_e, of the CMPs.[38,40,61] These CMPs induce downstream intracellular signaling, which we first model via a Local Excitation Global Inhibition (LEGI) model.[62] The LEGI represents one of the simplest yet most comprehensive mathematical models for cell signaling.[63,64] The LEGI model computes an activator (A), an inhibitor (I), and a response element (R), which represents intracellular signals, small GTPases such as Rac and Cdc42, that activate the cell front through actin filament polymerization. To account for the actin polymerization against the cell membrane we follow well established models.[65] Migration is computed by a classical active gel model,[66,67] which is coupled with the signaling model to modify the actomyosin network velocity, v^F, and the actin polymerization at the cathodal and anodal fronts, v_p, which eventually dictate the migration direction and velocity of the cell.

To analyze electrotaxis through our computational model, we initially define an unpolarized state of the cell, i.e., the density of CMPs, intracellular signals, actin, and myosin are homogeneously distributed along the cell. The cell expands symmetrically as previously described[67] until we stimulate the cell with a physiological EF of 120 mV/mm at t = 180s (Figure 2). We first analyze the polarization of CMPs as the first responders to the externally applied EF. We use an electromigration model to evaluate the redistribution of CMPs. We use values of the ζ-potentials of the membrane surface in fibroblasts and mesenchymal stem cells of ≈ -60mV,[45] comprising the behavioral characteristics of most cell types, which have high negative ζ-potentials. In terms of the CMPs, we first focus on EGFR because it has been shown repetitively as one of the main extracellular components involved in electrotaxis.[22,34,68] The ζ-potential of EGFR is ≈ -9.24 mV.[69] The electrophoretic forces alone would make the EGFRs move with a velocity of -1.5 nm/s (toward the anode, Equation S2). However, the additional presence of the electroosmotic flow makes the negatively charged EGFRs accumulate cathodally with an electromobility velocity of 6 nm/s (Figure 2A; Equation 1).

The polarization of EGFRs induces a cascade of intracellular signals that we account for with an LEGI signaling model. First, the accumulation of EGFR at the cathodal side activates PI3K pathways, which activates the responders (e.g., small GTPases Rac1 and Cdc42) (Figure 2B). This signaling process has two main effects on the migration behavior of the cell. First, the actin polymerization velocity increases in those regions where EGFR, and consequently PI3K, Rac1, and Cdc42, accumulate. The polarization of Rac1 induces an equal polarization but in opposite directions in RhoA[70,71] and, consequently, in myosin activity, which results in a backward retrograde flow (Figure 2C). The retrograde flow drags the actomyosin network, which further increases the front-rear polarization in a positive feedback loop (Figures 2D and 2E). The balance between the actin polymerization velocity and the retrograde flow velocities at the cell fronts establishes the directed migration of the cell to the cathode

Table 2. Table of model variables and occurrence

Variable	Definition	Occurrence
v^F	Retrograde Flow velocity	Figures 1 and 2, Equation 8
v_p	Polymerization Velocity	Figures 1 and 2, Equation 9
v	Migration velocity of the cell	Figures 1, 2, 3, and 4, Equation 10
v_e	Electromotility Velocity of the CMPs	Figure 3, Equations 3 and 4
$\rho_\pm$	Density of CMPs (Charged membrane proteins)	Figure 2, Equation 4
R	Density of the responder in the LEGI model	Figure 2, Equations 5, 6, and 7
ρ^F	Density of Actin	Figure 2, Equations 11 and 12
ρ^M	Density of Myosin	Figure 2, Equations 13 and 14
ζ_1	Zeta Potential of the CMP	Equation 3 and Equations S2–S4
ζ_2	Zeta Potential of the cell surface	Equation 3 and Equation S1
G, G^i	Concentrations of active and inactive form of GTPases respectively	Equations 1 and 2

(Figure 2F) with a steady-state velocity of 0.014 μ m/s, in agreement with the velocity and direction of cell migration[22,23] (Figure 2J).

Moreover, cells may also be initially polarized, migrating in a given direction, or previous stimuli could be present. To address this case, we take the same EF case above (Figure 2) and consider this cathodal migration as a natural polarization or polarization due to any stimuli. Then, we shift the EF direction to address how an EF can reverse the migration direction to that initially polarized cell (Figure S8B). Our results show how the EF is capable to repolarizing the CMPs, the underlying signals, and the motile machinery. For further analysis of how multiple signals can compete with each other, we refer to Betorz et al.[67]

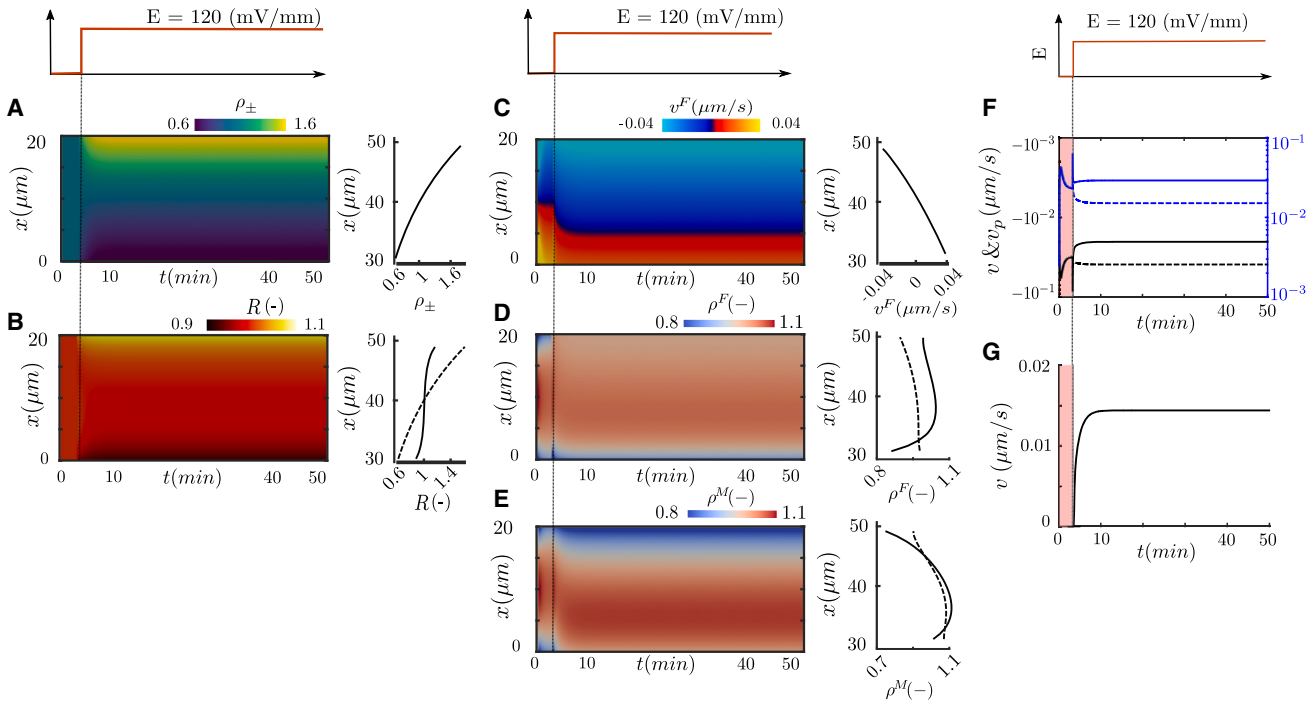

Figure 2. Computational results of a cell stimulated with an EF of 120 mV/mm with ζ-potential difference of 50.76 *mV*

(A–E) Kymograph of model variables along the initial cell length (Y axis) over time (X axis): CMPs polarization (A), intracellular signals (B), retrograde flow (C), actin (D), and myosin (E) densities. At the right of each panel, the CMPs, the intracellular signals (responder, solid line, and activator, dash line), the retrograde flow, actin (F-actin, solid line, G-actin, dash line) and myosin densities (bound, solid line, unbound, dash line) are shown at steady state; Retrograde flow (solid), blue and black at the cathodal and anodal sides of the cell, respectively, and polymerization velocity (dash), black and blue at the cathodal and anodal sides of the cell, respectively (F); Migration velocity of the cell (G). Color bars are differentiated by transmembrane, internal signal and actomyosin network variables.

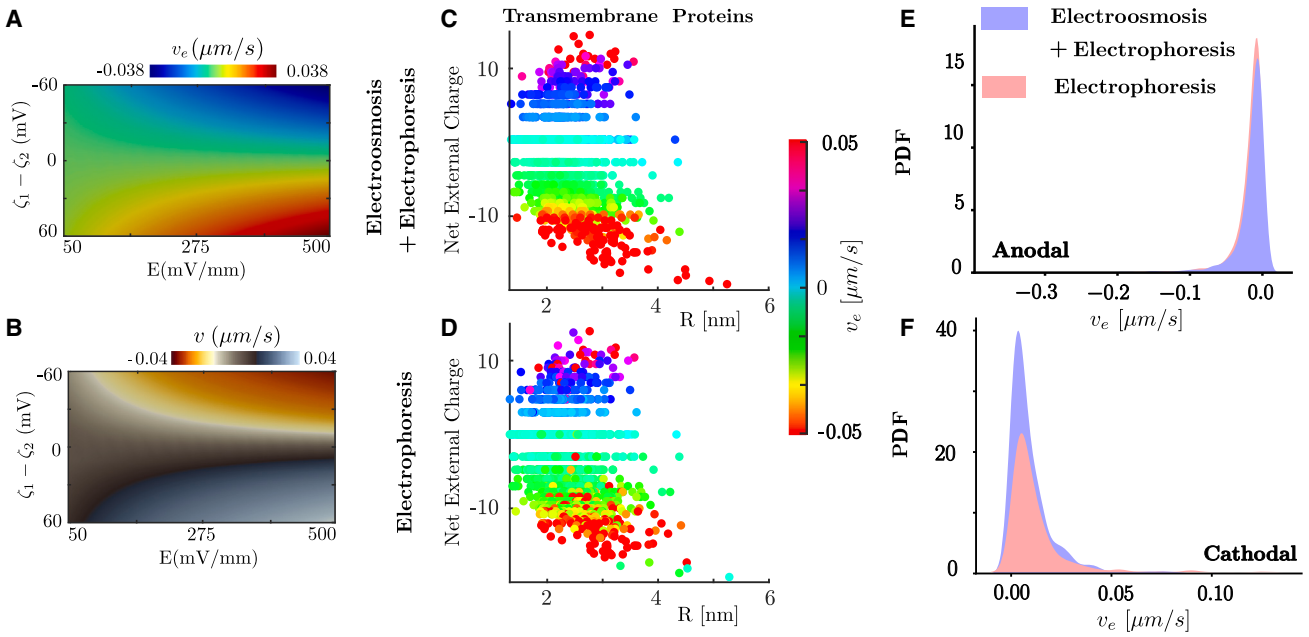

Figure 3. Effect of an electric field in CMPs

Color map of the model results for (A) electromotility and (B) migration velocities. The results are computed for a ζ-potential difference in a range of -60 to 60 mV and an EF stimulus in a range of 50–500 mV/mm.

(C) Results of electromigration velocities on transmembrane proteins when electroosmosis and electrophoresis are active and (D) when electroosmotic flows have been canceled.

(E and F) For those proteins that electromigrate toward the cathode and the anode, we compute the PDF for the control (electro-osmosis + electrophoresis) and the modified system (only electrophoresis). The PDFs have been normalized by using multivariable analysis, meaning that the sum of the areas for the two distributions adds to 1—this helps visualize which case dominates in that particular velocity regime.

In summary, our model integrates all modules involved in the cascade of events that triggers electrotaxis. It pinpoints the fundamental role of the ζ-potential in the response of CMPs to an EF (EGFR in this case), describes the role of the polarization of the CMPs in the downstream regulation of PI3K and GTPases and the consequent polarization of the intracellular forces that control cell migration. The model reproduces the polarization of EGFR, PI3K, and small GTPases toward the cathode as previously described.[22,23,34]

ζ-potential differences explain opposing electrotactic directions

As we showed above, the polarization of EGFR and the downstream signaling events polarize the cell toward the cathode. Although electrotaxis is ubiquitous across cell types and certain cell types migrate toward the cathode, others do it toward the anode as we described in the introduction. Based on an EGFR-centered model, as the main CMP involved in the sensing process, this would not be possible. However, there are other CMPs involved in downstream signals of the migratory machinery of the cell. Different CMPs, with different physical properties, have different ζ-potentials and sizes. Indeed, the sign of the ζ-potential difference should explain the polarization of the CMPs toward the cathode or the anode (see Equations 1 and 2) and, consequently, the cathodal and anodal migration, respectively.

Therefore, we analyze the effect of the ζ-potential differences in electrotaxis by considering hypothetical cells with a ζ-potential difference in a range of -60 to 60 mV exposed to a range of EFs between 50 and 500 mV/mm and compute the electromotility velocity of the CMPs (Figure 3A). These CMPs can then be responsible for the activation of downstream signals as described for EGFR above. Electromotility velocities increase as we increase the strength of the EF and the magnitude of the ζ-potential difference. Increasing values of ζ-potential differences and EF induce an increasing accumulation of CMPs toward the cathode ($\zeta_1 - \zeta_2 > 0$) or anode ($\zeta_1 - \zeta_2 < 0$).

Then, we compute the cell migration velocity for each combination of ζ-potential and EFs at steady-state. As expected, our results show a clear correlation between the sign of the ζ-potential difference and the direction of cell migration and between the magnitude of the ζ-potential difference and of the EF and the migration velocity of the cell (Figure 3B), as repetitively shown in the literature. Therefore, cells crowded by CMPs that result in ζ-potential differences of the same magnitude but opposite signs induce migration velocities of the same magnitude but opposite direction, i.e., cathodal and anodal electrotaxis (Figure 3B).

As one could have predicted, the model results suggest that the ζ-potential difference of cells, and consequently the electromotility of CMPs, may be responsible for the different electrotactic responses across cell types.

Track down CMPs responsible for electrotaxis

Then, we wonder what specific CMPs could match a specific ζ-potential difference and, consequently, could be responsible for anodal or cathodal migrations. To tackle this idea, we used a previous screening of the zebrafish keratocytes proteome to describe the electromigration of CMPs (see[40] for a complete description of the screening process and the physical properties of the proteins).

First, we compute the electromotility velocity v_e following Sarkar et al,[40] who assumed pure electrostatic forces without formation of an EDL around the CMPs, and we plot it as a function of the charge and equivalent radius of transmembrane proteins (Figure 3C). Our results show that 62% of transmembrane proteins redistribute toward the anode (Figures S2 and S3). All proteins that accumulate toward the anode have net negative extracellular charges, with an averaged mean charge of −6.11. For these proteins, electrophoretic forces are larger than the drag forces due to the cathodal electroosmotic flow. For cathodal accumulating proteins, 62.6% of transmembrane proteins have positive charges, meaning that electrophoretic and electroosmotic forces cooperate to drag proteins toward the cathode. In the cases with negative CMPs, the electroosmotic flow dominates, and the CMPs polarize toward the cathode. All proteins analyzed are provided as Data S1 with their physical properties and electromigration velocities. A statistical analysis is also shown in Figures S2 and S3.

Then, we identify proteins that may be implicated in downstream signals for cell migration. For those proteins that electromigrate toward the cathode, we found proteins participating in the EGFR transactivation/metalloproteases pathway (alpha-2A adrenergic receptor) and PI3K signaling (tyrosine-protein kinase STYK1), epithelial-mesenchymal transition (lysophosphatidic acid receptor 5b), and G protein-coupled receptors/Rho GTPases (sphingosine 1-phosphate receptor 1). In the list of anodal accumulating transmembrane proteins, we also found proteins participating in interrelated pathways that include EGFR transactivation/metalloproteases (type-1 angiotensin II receptor) and PI3K signaling (adiponectin receptor protein 2), epithelial-mesenchymal transition (TM2 domain-containing protein 1 precursor), integrin involvement (nuclear envelope integral membrane protein 2), G protein-coupled receptors/Rho GTPases (beta-2 adrenergic receptor), and metalloproteases (tetraspanin-12). Each CMP and the affecting signaling pathway is available in Data S2.

We also analyze v_e assuming the formation of an EDL around the CMPs as we did in previous sections (see for details on the v_e calculation). The results are qualitatively similar to the case in which the EDL is neglected. Now, only 52.9 % of transmembrane proteins redistribute toward the anode, with an averaged mean charge of − 6.97. For cathodal accumulating proteins, 50.8 % of transmembrane proteins have positive charges. Many of the above mentioned CMPs proteins implicated in downstream signals for cell migration were also found in this case. All proteins analyzed and the affecting signaling pathway of each CMP are available in Data S3 and Data S4 Finally, we look into CMPs However, the assumption that all CMPs may be dragged by the maximum electroosmotic flow velocity could be overestimated. Some proteins could have the core domains below that maximum velocity while others could have them above the Debye length and there are even different approaches to compute electrophoresis of CMPs based on the formation of the EDL. Moreover, solutions of higher viscosity than the value used here could create a much slower electroosmotic flow. To analyze the effect of these extreme scenarios, we recompute the electromigration of all CMPs without the electroosmotic flow (Figures 3D, S4C, and S4D). Our results show a preferential polarization of CMPs toward the anode because the electroosmotic flow, assisting the cathodal accumulation, is now canceled, both for the calculation of v_e assuming or neglecting the formation of the EDL. Now, the percentage of CMPs accumulating toward the anode for transmembrane proteins is 73.1% (Figure S3) when the EDL is neglected (same behavior is observed when the EDL is taken into account). We also plot the probability density function (PDF) of proteins accumulating in the cathode and the anode for these cases (Figures 3E, 3F, S4B, and S4D). Finally, we look into CMPs that electromigrated to the cathode in the control case but switched to the anode when the electroosmotic flow is removed. We find several proteins, such as the Galanin receptor 2b and the Tyrosine-protein kinase receptor Tie-2 when EDL around the CMPs is neglected, or the G protein coupled receptor 26 when the EDL is considered, that are implicated in different pathways of cell migration (highlighted in yellow in Data S2 and S4). Together, these results show simultaneous anodal and cathodal accumulation of transmembrane proteins involved in downstream signaling pathways of the motile machinery of the cell with different approaches in the calculation of the electromigration velocity.[40] Whether anodal or cathodal electrotaxis prevails will depend on the polarization of CMP, the following competition of signaling pathways, and the strength of these mechanisms that make either the anodal or cathodal electrotaxis win.

Intracellular signaling may explain opposing migration directions

Then, we wonder how this opposing redistribution of CMPs and, consequently, multiple stimuli for intracellular signaling impacts electrotaxis. To analyze this scenario, we increase the complexity of the signaling model. Instead of the LEGI model used above, we adopt a model that includes an explicit description of small GTPases of the rho family (Rac1, Cdc42, and RhoA), phosphoinositide kinases (PI3K and PI5K), and phosphoinositides (PI(4)P, PI(4,5) P_2, and PI(3,4,5) P_3, or PIP, PIP2, and PIP3, respectively) (see[72] for details). This approach allows us to impose stimuli for each pathway (rho GTPases, phosphoinositide kinases, and phosphoinositides) and analyze the feedback loops between them (Figure 4A). A complete description of these interactions and the full coupled system of partial derivative equations (PDEs) is described in STAR Methods.

Because we do not know all CMPs involved in the signaling process and how strongly they respond to the polarized CMPs, we explore mathematically different possibilities. We assume that there are two separate CMPs that can take values of the ζ-potential difference either 10 or -10 mV. To investigate possible cooperative and competing combinations of these stimuli, we assume that one of these CMPs induces the activation of PI3Ks and the other can activate Rac1 and Cdc42 through

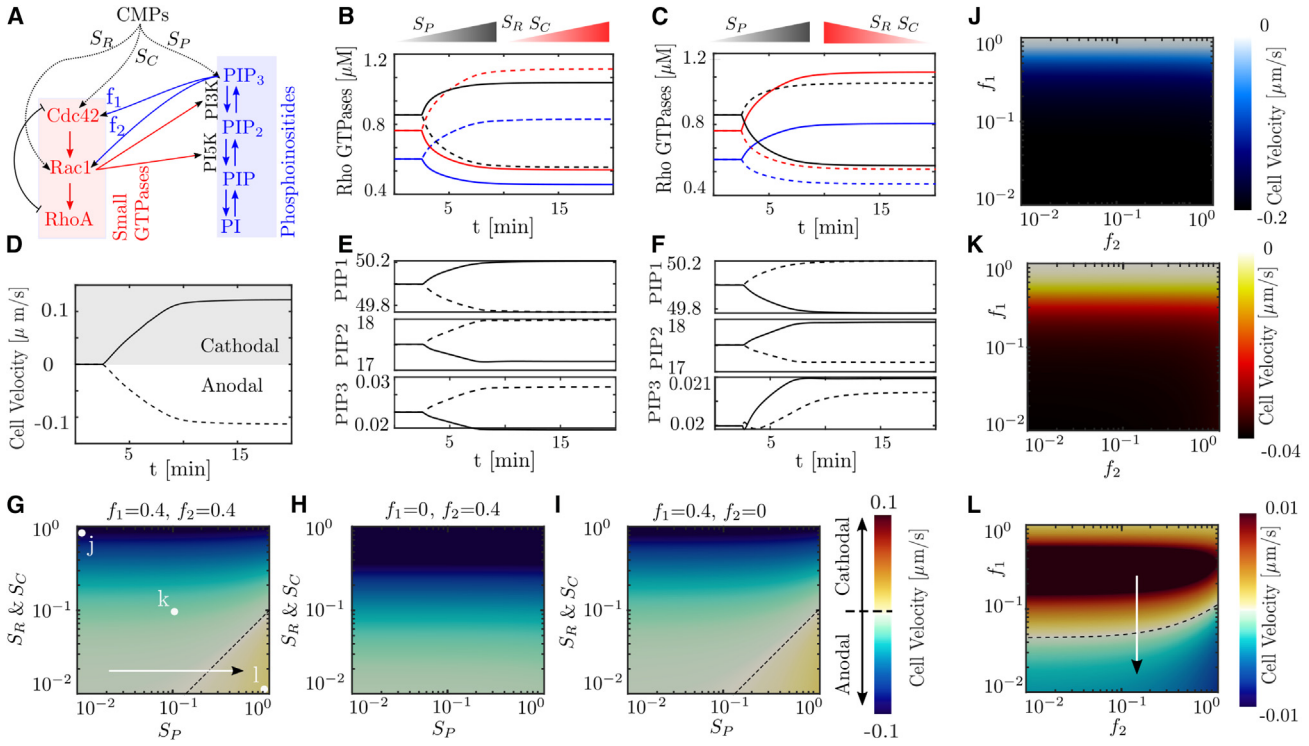

Figure 4. Effect of the CMPs polarization in the signaling network and migration of the cell

(A) Schematic representation of the signaling interactions. Arrows indicate positive feedback (activation) from one component to another. Tails indicate negative feedback (inactivation) of one component by another. f_1 and f_2 are the magnitudes of feedback for activating Cdc42 and Rac1 by PIP3. S_i are the strength of the signal from receptors to GTPases or PI3K.

(B–F) Two cases are shown, where the gradient of receptors that activates PI3K is always polarized toward the cathode (gray gradient) and the polarization of receptors that activate Rac1 and Cdc42 are toward the cathode (B and E) or the anode (C and F). (B and C) Evolution in time of Rac (blue), Cdc42 (red) and Rho (black), and PIPs (E and F) in the cathodal (dash) and anodal (solid) side of the cell are presented. (D) Cell migration velocity for the cases presented in (B–E) and (C–F). For the case presented in (B and C), we vary the strength of the stimulus S_P, S_R, and S_C in a normal feedback loop from PIP3 to Cdc42 and Rac1 (G), when no feedback loop to Cdc42 (H) and no feedback loop to Rac1 (I). For the three cases presented in (G) in points (J–L) we vary the strength of the feedback loop from PIP3 to Cdc42 and Rac1.

GEFs (Figure 4A). We compute the polarization of these two CMPs under the stimulus of an EF of 120 mV/mm (Figures 4B–4F), which produces anodal and/or cathodal accumulation of CMPs depending on the value of the ζ-potential difference.

Unless stated otherwise, we take the CMP that polarizes toward the cathode to activate PI3K in all our following simulations. In our control case, we assume that the other CMP, which activates Rac1 and Cdc42, also polarizes toward the cathode (Figures 4B and 4E). The accumulation of Cdc42 in the cathodal side of the cell induces a strong actin polymerization, that pushes the membrane forward and an accumulation of RhoA at the anodal side, that activates myosin activity and a cathodal-to-anodal retrograde flow (Figure S5). Eventually, the chain of cooperative positive feedback loops induces an electrotactic response toward the cathode with a migration velocity of 0.12 μ m/s (Figure 4D). Next, we consider that the CMPs responsible for activating Rac1 and Cdc42 polarize toward the anode, competing with the downstream signals of the cathodal PI3K polarization (Figures 4C and 4F). Our simulation shows that cells would migrate anodally with a velocity of -0.115 μ m/s (Figure 4D). These results indicate that direct activation of GTPases (Cdc42 and Rac1) and not PI3K seems to dominate the final polarization of the cell (Figures 4D, S6, and S7). Then, to understand the behavior of different cell types, we wonder how different values of the strength of the stimuli (S_R, S_C, and S_P) and the feedback loops from PIP3 to the GTPases (f_1 and f_2, Figure 4A) impact electrotaxis (Figures 4G–4I). We focus on the case where the CMPs responsible for PI3K and Cdc42 polarize in opposite directions. First, we vary the stimuli strength and keep the feedback from PIP3 toward Rac1 and Cdc42 (Figure 4G). Our results show that migration occurs preferentially toward the anode or, in other words, toward the Cdc42 polarization. However, cells migrate cathodally for ratios of $S_P/S_C \rangle 10$ following the PI3K polarization. If the feedback from PIP3 to Cdc42 is canceled, cells migrate anodally with higher velocity because the opposing stimulus coming from the PI3K polarization is inhibited (Figure 4H). Further, the inhibition of the feedback from PIP3 to Rac1 does not affect the migration velocity (Figures 4G and 4I), indicating the effect of Rac1 from the PIP3 activation is weak. These results suggest that changes in the activation strength of PIP3 have little effect on cell migration velocity and that activation of Cdc42 dominates over the activation from PI3K and Rac1.

To further understand how the feedback from PIP3 to Cdc42 and Rac1 may affect the signaling process,[72–74] we analyze the effect of their strength (Figures 4J–4L). We analyze 3 cases (see dots in Figure 4G) with different ratios of the stimuli strengths, S_R, S_C, and S_P. As shown before, the feedback strength from PIP3 to Rac1 does not affect the migration velocity of the cell for ratios S_R/S_P that initially induced anodal migration (Figures 4J and 4K). If the feedback strength from PIP3 to Cdc42 is enhanced, the migration velocity also increases but does not change the migration direction (Figures 4J and 4K). However, for ratios of S_R/S_P that induce migration toward the PI3K accumulation (point l, Figure 4G), the migration direction strongly depends on the feedback strength from PIP3 to Cdc42 (Figure 4L). Inhibition of the feedback from PIP3 to Cdc42 will shift the migration direction toward the anode, where Cdc42 polarizes, by recovering the effect of the direct activation of the GTPases.

Together, these results unveil the complex connections between the stimuli induced by the polarized CMPs and the strength of the downstream signaling pathways. Our results show how different strengths of PIPs to GTPases feedback loops and of the stimuli induced by the CMPs electro-migration can induce anodal and cathodal electrotaxis.

Electrotactic control by cellular manipulation

Next, we wonder how we could manipulate cells to engineer a specific response to enhance, arrest, or shift the electrotaxis direction. To do so, we look back into the main ingredients involved in electrotaxis. Cell motility can be directly modified by myosin activity, actin polymerization, or adhesion manipulations, e.g., blebbistatin, CK-666, or talin knockouts, respectively. We showed through mathematical models the effect of this intracellular manipulation on cell migration.[65,75] However, these are not unique to electrotaxis.

Electrotaxis must be directly coordinated by the polarization of CMPs and the downstream signaling pathways. Therefore, one could induce changes in the electromigration direction of CMPs. The literature has proposed different ways of such manipulation, which become clear when we look at Equation 1. One option is to modify the viscosity of the medium, which reduces the electroosmotic flow as demonstrated above (Figure 3). This effect has been demonstrated in cells cultured in low molecular weight polymers.[76] Another option is to change the charge amount of the CMPs by modifying the pH of the medium[38,40] or by glycosylation. Glycosylation has been shown to shift the cathodal electromigration of CMPs to the anodal.[40] For small negative values of cell surface ζ-potential, the electroosmotic flow due to the negative cell surface charge pushes the CMPs toward the cathode. When the CMP charge becomes more negative, presumably the negative charge generates a larger electrophoretic attraction toward the anode and, therefore, it can compensate for the drag forces toward the cathode. However, the effects on the migration of CMPs by such putative electrophoretic force are complicated by the electroosmotic effect and the ζ-potential variation, making its mathematical modeling of this particular aspect unfeasible.

Finally, we can also infer the signaling pathways to modify electrotaxis. Let us assume a cell that shows Cdc42 polarization and migration toward the cathode but PIP3 polarization is toward the anode (Figures 4C and 4F). Migration inhibition would be consistent with a system in which a strong GTPases polarization does not receive enough feedback activation from PIP3, whether PI3K sufficiently activates PIP3 or not (point j, Figures 4G and 4J). These results suggest the feedback from PIP3 to Cdc42 as a key mediator in inhibiting or enhancing electrotaxis. There are two options to explain reversing electrotaxis direction. We observe electrotaxis toward the Cdc42 accumulation in a system where the activation of GTPases and PI3K is weak. If we then enhance PI3K activation, which then directly feedback to PIP3, Cdc42, and Rac1, we would overrule the direct Cdc42 activation at the anodal side and promote cathodal accumulation (Figure 4G, white arrow). Second, in such manipulated or endogenous cases of strong PI3K activation (point l, Figure 4G), we could again reverse the migration direction either by inhibiting the PIP3 feedback to Cdc42 (Figure 4L, white arrow). It is key to note that, when the polarization of all CMPs is aligned toward the same side of the cell, we cannot find any signaling manipulation that can reverse migration direction.

One widely reported signaling manipulation consists of blocking PI3K expression,[16,24] which reduces the PIP2 to PIP3 activation and, consequently, feedback to Rac1 and Cdc42. Although most studies have shown a reduction in migration velocity, there are reports of electrotactic inhibition, no change in the electrotaxis response, or even a shift in the migration direction.[26,77] Our model conceptualizes most of these observations (point j, Figures 4J–4L), as we have described in the previous paragraph. These opposing responses would depend on the strength of all stimuli and feedback loops. To analyze the blocking PI3K expression, we reduce the strengths S_R and S_C to zero so that the CMPs polarization does not induce a direct polarization of Rac1 or Cdc42. Rac1 or Cdc42 can still be activated by PIP3 feedback. We compute the migration velocity with the baseline value of k^*_{pi3k} and with a reduction of 90%. Our results show that migration velocity reduces by 93% (Figure S1), consistently with the usual observation of migration inhibition.

DISCUSSION

The control on-demand of cell migration has huge implications in cancer, wound healing, and tissue engineering. Among other external cues, an EF represents a stable and programmable signal to control cell motility.[13] Although electrotaxis happens in a multitude of cellular systems, it is expressed with important differences. Some cell types migrate toward the anode while others do it toward the cathode. To precisely control electrotaxis, we must understand the fundamental mechanisms that enable electrotaxis across cell types.

By adopting a minimal model of cell migration[67] and extending it with electromigration of cell membrane receptors and signaling pathways implicated in cell motility, we have proposed a complete computational model of electrotaxis. To this end, we first used the physical values of EGFR, which has been implicated in electrotaxis,[22,34,35,68] to model the whole chain of events involved in electrotaxis. We show that EGFR polarizes cathodally, as shown before in the literature. We also show the cathodal accumulation of downstream signals, e.g., PI3K, which is also described in the literature,[16,24,26,77] and finally the polarization

of the motile machinery of the cell to eventually lead to cathodal migration, as shown in these previous works. Next, we wonder how it is then possible that some cells still migrate to the anode. We argue that other signaling proteins should be implicated in electrotaxis. To prove this hypothesis, we used the zebrafish proteome and computed the electromigration of each of the membrane proteins. Our results showed that an approximate even number of proteins would polarize anodally and cathodally, and we hypothesize that some of the proteins that polarized toward the anode could be responsible for anodal migration. To further prove this hypothesis, we simulate cases in which two hypothetical proteins would polarize toward either the same electrode or opposite ones. We showed that competing stimuli could induce anodal electrotaxis. These theoretical results establish guidelines and tools to reduce the number of proteins to study and even to address which ones are candidates for electrotaxis. We hope that future work can use these guidelines to analyze the behavior of specific cell lines.

We also looked for specific membrane proteins that may be involved in electrotaxis as key regulators in cell migration.[38,40] When we looked into the zebrafish's proteome, we identified transmembrane proteins involved in the downstream signaling pathways of electrotaxis that accumulated anodally and cathodally and, therefore, they may compete to establish a specific migration direction. Our results indicate that individual CMPs electromigrate cathodally and anodally and that they may predominately accumulate anodally if electroosmotic flows are reduced, or if the charge amount is increased. Indeed, we also identified a few proteins implicated in cell motility, such as EGFRs and G protein coupled receptors, that show cathodal polarization in a control set-up but can migrate anodally if the electroosmotic flow is canceled. But what could happen if, as we demonstrate, multiple stimuli compete to determine the final cell polarization? With our computational model, we showed that the opposed polarization of membrane receptors can trigger downstream competing signaling pathways and that, depending on where and at what strength receptors polarize, the prevailing signal will make cells migrate anodally or cathodally. This activation strength can be cell-type dependent, and the downstream signaling competition between different activation pathways may explain antagonistic responses in electrotaxis. Our results, in addition to replicating previous experimental findings, provide a mechanistic rationale for how different cell types may exhibit anodal or cathodal migration.

These conclusions lead us to propose future experimental work, that lies beyond the scope of this work. Most of the data today usually reduces to one specific receptor and, in some cases, the studies extend to the analysis of one other intracellular signal, for example, PIP3 or PI3K. First, a detailed proteome analysis of each cell line should be performed, followed by the electromotility study of each protein and their corresponding downstream signaling pathways for cell migration. Based on our analysis, differences in cellular responses, such as migration velocities or time to respond to an electric stimulus, should respond to differences in activation strengths and the feedback loops between GTPases and PIPs. We strongly suggest that the next steps should focus on a consistent analysis of how all these signals (Rac1, Cdc42, RhoA, PI3K, PI5K, PIP, PIP2, and PIP3), and not only one of them, polarize under the EF. This extensive data analysis would tell us how these feedback loops occur, which should uniquely determine the electrotactic mechanics for a specific cell line, providing a case-by-case answer to the response of cells to an external EF.

Here, we have made use of the zebrafish proteome to describe the mechanisms and competing signaling pathways that may be involved in electrotaxis. It has been suggested that most cell types share around 70–80% of their proteome[78,79] and the remaining 20–30% differentially expressed between cell types are due to tissue specialization and environmental responses. Future work should focus on a detailed proteome analysis of cell types that would allow us to check the differences in that 20–30% and show what CMPs polarize to what side, study their implication in signaling and migratory pathways and provide a close potential candidate to predict directional migration in electrotaxis. Related to the cell line specificity, we chose a very complete signaling model that has been successfully applied to reproduce the behavior of certain cell types. However, we could also use other signaling models that may reproduce more accurately certain cell types. Future work on specific cell types will have to analyze which one of such models better reproduces the behavior of each cell line (see[64] for details on signaling model comparison). Our computational model stands as a potential tool to guide future experimental research in electrotaxis. To this end, we present an online platform for the scientific community (uploaded in the MATLAB Central File Exchange) that, upon providing the physical properties of the membrane proteins and the EF strength yields the distribution of the proteins, the Rho-GTPases, PIPs, and phosphoinositides, the myosin and actin distribution and the migration velocity of the cell. Future work on coupling our platform with multicellular models[80] and specialized approaches to consider other signaling models[64] and effects on amount of receptors[81] should be analyzed.

Limitations of the study

Our model reduces and rationalizes electrotaxis in terms of the final polarization of the actomyosin network. However, other mechanisms could also be involved in electrotaxis. An EF also activates voltage-gated ion channels. The cell membrane depolarization would lead to the elevation in intracellular ion concentration. Ca^{2+}, Na^{+}, and K^{+} channels have been directly implicated in electrotaxis.[82,83] Indeed, one of the immediate effects in terms of cellular response to EF stimulation is the increase in intracellular Ca^{2+}.[84–86] Some previous works have looked into how ion fluxes and pH affect cell migration,[87,88] and further work coupling such approaches with electromigration of ion channels should be conducted in the future. Even though some previous data have ruled out this contribution to electrotaxis, it would be interesting to develop a computational model to analyze these cases and propose possible sensing and transductive mechanisms of electrotaxis through such electrochemical regulation events. We have also assumed that CMPs electromigrate in isolation. However, multiple CMPs, including EGFR, may coalesce to form rafts with a total negative charge larger than the ζ-potential of the cell membrane which would result in a negative ζ-potential difference. In that case, the stronger electrophoretic attraction will result in anodal migration, which has

been reported in literature.[45] Moreover, when we analyzed the electromigration of the zebrafish keratocyte proteome, we computed the electromigration velocity neglecting and incorporating the formation of the EDL around the CMPs.[40,61,89] However, both approaches provided similar results, which further show that CMPs can polarize anodally and cathodally. Probably, neither of these two approaches reproduce the actual electromigration of CMPs, which have geometries much different than the perfect spheres that most studies consider. Moreover, if we assume that CMPs also contribute to the zeta potential of the cell surface, but CMPs polarize along it, there would be locations of the cell surface with different values of zeta potential, which would modify the zeta potential locally. We have not studied this scenario. These are important considerations that deserve further investigation in the future. Perhaps, there are even other mechanisms that we have not yet thought about and, therefore, the experimental and theoretical work on electrotaxis will still need to work together. There is also an obvious limitation in our model due to the 1D approach we chose. This framework limits the analysis of important cases in electrotaxis, such as cells that elongate perpendicular to the EF[90,91] or cells that migrate following complex EF distributions.[13,17] Well-established numerical methods could be used in the future to address electrotaxis in higher dimensions.[92,93]

Finally, electrotaxis has been also described for cell aggregates.[13,17,18,94,95] Integrating dynamics from single cells into models of cell aggregates[80] should also be targeted to reveal the interplay of intra- and extracellular sensing mechanisms in tissue electrotaxis.

RESOURCE AVAILABILITY

Lead contact

Further information and requests for resources should be directed to the lead contact, Pablo Sáez (pablo.saez@upc.edu).

Materials availability

This study did not generate new material.

Data and code availability

- All data reported in this paper will be shared by the lead contact upon request.
- All original code has been deposited at the MATLAB Central File Exchange and is publicly available as of the date of publication.
- Any additional information required to reanalyze the data reported in this paper is available from the lead contact upon request.

ACKNOWLEDGMENTS

PS acknowledges the support of the Spanish Ministry of Science and Innovation (Grant PID2022-142178NB-I00 funded by MCIN/AEI/10.13039/501100011033/FEDER, UE). S.K. was supported by the Spanish Ministry of Economy and Competitiveness (Grant number: PRE2020-095851). C.R. and F.T. were supported by the Spanish Ministry of Science and Innovation (Grant PID2020-115910RB-I00). We thank Y. Takada and K. Zhu for their insightful discussions.

AUTHOR CONTRIBUTIONS

P.S. and M.Z. designed the study. P.S. and S.K. performed the simulations. P.S. wrote the paper. F.T. and C.R. performed the proteomic analysis. All authors analyzed the data and critically reviewed the paper.

DECLARATION OF INTERESTS

The authors declare no competing interests.

STAR★METHODS

Detailed methods are provided in the online version of this paper and include the following:

- KEY RESOURCES TABLE
- METHOD DETAILS
  - Electromotility of charged membrane components
  - Signaling pathways and mathematical model
  - Polarization of signaling cues by the LEGI model
  - Polarization of signaling cues by a GTPases model
  - Mechanical model of the actomyosin network
  - Kinetics of the cell fronts
  - Transport of the actomyosin network
  - Numerical solution of the problem and model parameters
  - Proteomic analysis
- QUANTIFICATION AND STATISTICAL ANALYSIS

SUPPLEMENTAL INFORMATION

Supplemental information can be found online at https://doi.org/10.1016/j.isci.2025.112329.

Received: August 8, 2024
Revised: October 1, 2024
Accepted: March 28, 2025
Published: April 2, 2025

REFERENCES

1. Friedl, P., and Gilmour, D. (2009). Collective cell migration in morphogenesis, regeneration and cancer. Nat. Rev. Mol. Cell Biol. *10*, 445–457. https://doi.org/10.1038/nrm2720.
2. Mayor, R., and Etienne-Manneville, S. (2016). The front and rear of collective cell migration. Nat. Rev. Mol. Cell Biol. *17*, 97–109. https://doi.org/10.1038/nrm.2015.14.
3. Van Helvert, S., Storm, C., and Friedl, P. (2018). Mechanoreciprocity in cell migration. Nat. Cell Biol. *20*, 8–20. https://doi.org/10.1038/s41556-017-0012-0.
4. Van Haastert, P.J.M., and Devreotes, P.N. (2004). Chemotaxis: signalling the way forward. Nat. Rev. Mol. Cell Biol. *5*, 626–634. https://doi.org/10.1038/nrm1435.
5. Sunyer, R., and Trepat, X. (2020). Durotaxis. Curr. Biol. *30*, R383–R387. https://doi.org/10.1016/j.cub.2020.03.051.
6. Shellard, A., and Mayor, R. (2021). Durotaxis: The hard path from in vitro to in vivo. Dev. Cell *56*, 227–239. https://doi.org/10.1016/j.devcel.2020.11.019.
7. Butcher, D.T., Alliston, T., and Weaver, V.M. (2009). A tense situation: forcing tumour progression. Nat. Rev. Cancer *9*, 108–122. https://doi.org/10.1038/nrc2544.
8. Levin, M. (2009). Bioelectric mechanisms in regeneration: Unique aspects and future perspectives. Semin. Cell Dev. Biol. *20*, 543–556. https://doi.org/10.1016/j.semcdb.2009.04.013.
9. Langer, R., and Tirrell, D.A. (2004). Designing materials for biology and medicine. Nature *428*, 487–492. https://doi.org/10.1038/nature02388.
10. Wegst, U.G.K., Bai, H., Saiz, E., Tomsia, A.P., and Ritchie, R.O. (2015). Bioinspired structural materials. Nat. Mater. *14*, 23–36. https://doi.org/10.1038/nmat4089.
11. McCaig, C.D., Rajnicek, A.M., Song, B., and Zhao, M. (2005). Controlling Cell Behavior Electrically: Current Views and Future Potential. Physiol. Rev. *85*, 943–978. https://doi.org/10.1152/physrev.00020.2004.

12. Cortese, B., Palamà, I.E., D'Amone, S., and Gigli, G. (2014). Influence of electrotaxis on cell behaviour. Integr. Biol. *6*, 817–830. https://doi.org/10.1039/c4ib00142g.

13. Zajdel, T.J., Shim, G., Wang, L., Rossello-Martinez, A., and Cohen, D.J. (2020). SCHEEPDOG: Programming Electric Cues to Dynamically Herd Large-Scale Cell Migration. Cell Syst. *10*, 506–514.e3. https://doi.org/10.1016/j.cels.2020.05.009.

14. Yan, X., Han, J., Zhang, Z., Wang, J., Cheng, Q., Gao, K., Ni, Y., and Wang, Y. (2009). Lung cancer A549 cells migrate directionally in DC electric fields with polarized and activated EGFRs. Bioelectromagnetics *30*, 29–35. https://doi.org/10.1002/bem.20436.

15. Patel, N., and Poo, M.M. (1982). Orientation of neurite growth by extracellular electric fields. J. Neurosci. *2*, 483–496. https://doi.org/10.1523/JNEUROSCI.02-04-00483.

16. Zhao, M., Song, B., Pu, J., Wada, T., Reid, B., Tai, G., Wang, F., Guo, A., Walczysko, P., Gu, Y., et al. (2006). Electrical signals control wound healing through phosphatidylinositol-3-OH kinase- and PTEN. Nature *442*, 457–460. https://doi.org/10.1038/nature04925.

17. Cohen, D.J., Nelson, W.J., and Maharbiz, M.M. (2014). Galvanotactic control of collective cell migration in epithelial monolayers. Nat. Mater. *13*, 409–417. https://doi.org/10.1038/nmat3891.

18. Zhang, Y., Xu, G., Wu, J., Lee, R.M., Zhu, Z., Sun, Y., Zhu, K., Losert, W., Liao, S., Zhang, G., et al. (2022). Regulation of RhoA GTP hydrolysis by the gtpase-activating proteins p190, p50RhoGAP, bcr, and 3BP-1. Biochemistry *25*, 5249–5257. https://doi.org/10.1016/j.isci.2022.105136.

19. Hotary, K.B., and Robinson, K.R. (1994). Endogenous Electrical Currents and Voltage Gradients in *Xenopus* Embryos and the Consequences of Their Disruption. Dev. Biol. *166*, 789–800. https://doi.org/10.1006/dbio.1994.1357.

20. Zhao, M. (2009). Electrical fields in wound healing-An overriding signal that directs cell migration. Semin. Cell Dev. Biol. *20*, 674–682. https://doi.org/10.1016/j.semcdb.2008.12.009.

21. Fang, K.S., Ionides, E., George, O., Nuccitelli, R., and Rivkah Isseroff, R. (1999). Epidermal growth factor receptor relocalization and kinase activity are necessary for directional migration of keratinocytes in DC electric fields. J. Cell Sci. *112*, 1967–1978. https://doi.org/10.1242/jcs.112.12.

22. Zhao, M., Dick, A., Forrester, J.V., and McCaig, C.D. (1999). Electric field-directed cell motility involves up-regulated expression and asymmetric redistribution of the epidermal growth factor receptors and is enhanced by fibronectin and laminin. Mol. Biol. Cell *10*, 1259–1276. https://doi.org/10.1091/mbc.10.4.1259.

23. Zhao, M., Pu, J., Forrester, J.V., and McCaig, C.D. (2002). Membrane lipids, EGF receptors, and intracellular signals colocalize and are polarized in epithelial cells moving directionally in a physiological electric field. FASEB J. *16*, 857–859. https://doi.org/10.1096/fj.01-0811fje.

24. Meng, X., Arocena, M., Penninger, J., Gage, F.H., Zhao, M., and Song, B. (2011). PI3K mediated electrotaxis of embryonic and adult neural progenitor cells in the presence of growth factors. Exp. Neurol. *227*, 210–217. https://doi.org/10.1016/j.expneurol.2010.11.002.

25. Zhao, S., Zhu, K., Zhang, Y., Zhu, Z., Xu, Z., Zhao, M., and Pan, T. (2014). ElectroTaxis-on-a-Chip (ETC): an integrated quantitative high-throughput screening platform for electrical field-directed cell migration. Lab Chip *14*, 4398–4405. https://doi.org/10.1039/C4LC00745J.

26. Sun, Y.H., Sun, Y., Zhu, K., Reid, B., Gao, X., Draper, B.W., Zhao, M., and Mogilner, A. (2018). Electric fields accelerate cell polarization and bypass myosin action in motility initiation. J. Cell. Physiol. *233*, 2378–2385. https://doi.org/10.1002/jcp.26109.

27. Sun, Z., Costell, M., and Fässler, R. (2019). Integrin activation by talin, kindlin and mechanical forces. Nat. Cell Biol. *21*, 25–31. https://doi.org/10.1038/s41556-018-0234-9.

28. Zhu, K., Takada, Y., Nakajima, K., Sun, Y., Jiang, J., Zhang, Y., Zeng, Q., Takada, Y., and Zhao, M. (2019). Expression of integrins to control migration direction of electrotaxis. FASEB J. *33*, 9131–9141. https://doi.org/10.1096/fj.201802657r.

29. Zhao, M., Bai, H., Wang, E., Forrester, J.V., and McCaig, C.D. (2004). Electrical stimulation directly induces pre-angiogenic responses in vascular endothelial cells by signaling through VEGF receptors. J. Cell Sci. *117*, 397–405. https://doi.org/10.1242/jcs.00868.

30. Pu, J., McCaig, C.D., Cao, L., Zhao, Z., Segall, J.E., and Zhao, M. (2007). EGF receptor signalling is essential for electric-field-directed migration of breast cancer cells. J. Cell Sci. *120*, 3395–3403. https://doi.org/10.1242/jcs.002774.

31. Wu, D., Ma, X., and Lin, F. (2013). DC Electric Fields Direct Breast Cancer Cell Migration, Induce EGFR Polarization, and Increase the Intracellular Level of Calcium Ions. Cell Biochem. Biophys. *67*, 1115–1125. https://doi.org/10.1007/s12013-013-9615-7.

32. Zhao, Z., Watt, C., Karystinou, A., Roelofs, A.J., McCaig, C.D., Gibson, I.R., and De Bari, C. (2011). Directed migration of human bone marrow mesenchymal stem cells in a physiological direct current electric field. Eur. Cell. Mater. *22*, 344–358. https://doi.org/10.22203/ecm.v022a26.

33. Huang, C.-W., Cheng, J.-Y., Yen, M.-H., and Young, T.H. (2009). Electrotaxis of lung cancer cells in a multiple-electric-field chip. Biosens. Bioelectron. *24*, 3510–3516. https://doi.org/10.1016/j.bios.2009.05.001.

34. Wang, C.-C., Kao, Y.-C., Chi, P.-Y., Huang, C.-W., Lin, J.-Y., Chou, C.-F., Cheng, J.-Y., and Lee, C.-H. (2011). Asymmetric cancer-cell filopodium growth induced by electric-fields in a microfluidic culture chip. Lab Chip *11*, 695–699. https://doi.org/10.1039/C0LC00155D.

35. Tsai, H.-F., Huang, C.-W., Chang, H.-F., Chen, J.J.W., Lee, C.-H., and Cheng, J.-Y. (2013). Evaluation of EGFR and RTK Signaling in the Electrotaxis of Lung Adenocarcinoma Cells under Direct-Current Electric Field Stimulation. PLoS One *8*, e73418. https://doi.org/10.1371/journal.pone.0073418.

36. Lyon, J.G., Carroll, S.L., Mokarram, N., and Bellamkonda, R.V. (2019). Electrotaxis of Glioblastoma and Medulloblastoma Spheroidal Aggregates. Sci. Rep. *9*, 5309. https://doi.org/10.1038/s41598-019-41505-6.

37. Mossop, B.J., Barr, R.C., Zaharoff, D.A., and Yuan, F. (2004). Electric fields within cells as a function of membrane resistivity-a model study. IEEE Trans. NanoBioscience *3*, 225–231. https://doi.org/10.1109/TNB.2004.833703.

38. Allen, G.M., Mogilner, A., and Theriot, J.A. (2013). Electrophoresis of cellular membrane components creates the directional cue guiding keratocyte galvanotaxis. Curr. Biol. *23*, 560–568. https://doi.org/10.1016/j.cub.2013.02.047.

39. McCaig, C.D., Song, B., and Rajnicek, A.M. (2009). Electrical dimensions in cell science. J. Cell Sci. *122*, 4267–4276. https://doi.org/10.1242/jcs.023564.

40. Sarkar, A., Kobylkevich, B.M., Graham, D.M., and Messerli, M.A. (2019). Electromigration of cell surface macromolecules in DC electric fields during cell polarization and galvanotaxis. J. Theor. Biol. *478*, 58–73. https://doi.org/10.1016/j.jtbi.2019.06.015.

41. Jékely, G., Sung, H.-H., Luque, C.M., and Rørth, P. (2005). Regulators of endocytosis maintain localized receptor tyrosine kinase signaling in guided migration. Dev. Cell *9*, 197–207. https://doi.org/10.1016/j.devcel.2005.06.004.

42. Fukata, M., Nakagawa, M., and Kaibuchi, K. (2003). Roles of Rho-family GTPases in cell polarisation and directional migration. Curr. Opin. Cell Biol. *15*, 590–597. https://doi.org/10.1016/S0955-0674(03)00097-8.

43. MacHacek, M., Hodgson, L., Welch, C., Elliott, H., Pertz, O., Nalbant, P., Abell, A., Johnson, G.L., Hahn, K.M., and Danuser, G. (2009). Coordination of Rho GTPase activities during cell protrusion. Nature *461*, 99–103. https://doi.org/10.1038/nature08242.

44. Ridley, A.J. (2015). Rho GTPase signalling in cell migration. Curr. Opin. Cell Biol. *36*, 103–112. https://doi.org/10.1016/j.ceb.2015.08.005.

45. Lin, B.J., Tsao, S.H., Chen, A., Hu, S.K., Chao, L., and Chao, P.H.G. (2017). Lipid rafts sense and direct electric field-induced migration.

Proc. Natl. Acad. Sci. USA *114*, 8568–8573. https://doi.org/10.1073/pnas.1702526114.

46. Footer, M.J., Kerssemakers, J.W.J., Theriot, J.A., and Dogterom, M. (2007). Direct measurement of force generation by actin filament polymerization using an optical trap. Proc. Natl. Acad. Sci. USA *104*, 2181–2186. https://doi.org/10.1073/pnas.0607052104.
47. Schreiber, C.H., Stewart, M., and Duke, T. (2010). Simulation of cell motility that reproduces the force-velocity relationship. Proc. Natl. Acad. Sci. USA *107*, 9141–9146. https://doi.org/10.1073/pnas.1002538107.
48. Wong, S., Guo, W.H., and Wang, Y.L. (2014). Fibroblasts probe substrate rigidity with filopodia extensions before occupying an area. Proc. Natl. Acad. Sci. USA *111*, 17176–17181. https://doi.org/10.1073/pnas.1412285111.
49. Small, J.V., Stradal, T., Vignal, E., and Rottner, K. (2002). The lamellipodium: where motility begins. Trends Cell Biol. *12*, 112–120. https://doi.org/10.1016/S0962-8924(01)02237-1.
50. Pollard, T.D., Blanchoin, L., and Mullins, R.D. (2000). Molecular Mechanisms Controlling Actin Filament Dynamics in Nonmuscle Cells. Annu. Rev. Biophys. Biomol. Struct. *29*, 545–576. https://doi.org/10.1146/annurev.biophys.29.1.545.
51. Cramer, L.P. (1997). Molecular mechanism of actin-dependent retrograde flow in lamellipodia of motile cells. Front. Biosci. *2*, d260–d270.
52. Pantaloni, D., Boujemaa, R., Didry, D., Gounon, P., and Carlier, M.F. (2000). The Arp2/3 complex branches filament barbed ends: functional antagonism with capping proteins. Nat. Cell Biol. *2*, 385–391. https://doi.org/10.1038/35017011.
53. Pollard, T.D., and Cooper, J.A. (2009). Actin, a central player in cell shape and movement. Science *326*, 1208–1212.
54. Parsons, J.T., Horwitz, A.R., and Schwartz, M.A. (2010). Cell adhesion: integrating cytoskeletal dynamics and cellular tension. Nat. Rev. Mol. Cell Biol. *11*, 633–643. https://doi.org/10.1038/nrm2957.
55. Vicente-Manzanares, M., Choi, C.K., and Horwitz, A.R. (2009). Integrins in cell migration - the actin connection. J. Cell Sci. *122*, 1473. https://doi.org/10.1242/jcs.052894.
56. Chan, C.E., and Odde, D.J. (2008). Traction dynamics of filopodia on compliant substrates. Science *322*, 1687–1691. https://doi.org/10.1126/science.1163595.
57. Elosegui-Artola, A., Oria, R., Chen, Y., Kosmalska, A., Pérez-González, C., Castro, N., Zhu, C., Trepat, X., and Roca-Cusachs, P. (2016). Mechanical regulation of a molecular clutch defines force transmission and transduction in response to matrix rigidity. Nat. Cell Biol. *18*, 540–548. https://doi.org/10.1038/ncb3336.
58. Venturini, C., and Sáez, P. (2023). A multi-scale clutch model for adhesion complex mechanics. PLoS Comput. Biol. *19*, e1011250. https://doi.org/10.1371/journal.pcbi.1011250.
59. Ridley, A.J., Schwartz, M.A., Burridge, K., Firtel, R.A., Ginsberg, M.H., Borisy, G., Parsons, J.T., and Horwitz, A.R. (2003). Cell migration: Integrating signals from front to back. Science *302*, 1704–1709. https://doi.org/10.1126/science.1092053.
60. Devreotes, P., and Horwitz, A.R. (2015). Signaling Networks that Regulate Cell Migration. Cold Spring Harbor Perspect. Biol. *7*, a005959. https://doi.org/10.1101/cshperspect.a005959.
61. McLaughlin, S., and Poo, M.M. (1981). The role of electro-osmosis in the electric-field-induced movement of charged macromolecules on the surfaces of cells. Biophys. J. *34*, 85–93. https://doi.org/10.1016/S0006-3495(81)84838-2.
62. Levchenko, A., and Pablo, A. (2002). Iglesias. Models of Eukaryotic Gradient Sensing: Application to Chemotaxis of Amoebae and Neutrophils. Biophys. J. *82*, 50–63. https://doi.org/10.1016/S0006-3495(02)75373-3.
63. Devreotes, P.N., Bhattacharya, S., Edwards, M., Iglesias, P.A., Lampert, T., and Miao, Y. (2017). Excitable signal transduction networks in directed cell migration. Annu. Rev. Cell. Dev. Biol. *33*, 103–125. https://doi.org/10.1146/annurev-cellbio-100616-060739.
64. Jilkine, A., and Edelstein-Keshet, L. (2011). A comparison of mathematical models for polarization of single eukaryotic cells in response to guided cues. PLoS Comput. Biol. *7*, e1001121. https://doi.org/10.1371/journal.pcbi.1001121.
65. Mogilner, A., and Oster, G. (2003). Force generation by actin polymerization II: The elastic ratchet and tethered filaments. Biophys. J. *84*, 1591–1605. https://doi.org/10.1016/S0006-3495(03)74969-8.
66. Prost, J., Jülicher, F., and Joanny, J.-F. (2015). Active gel physics. Nat. Phys. *11*, 111–117. https://doi.org/10.1038/nphys3224.
67. Betorz, J., Bokil, G.R., Deshpande, S.M., Kulkarni, S., Araya, D.R., Venturini, C., and Sáez, P. (2023). A computational model for early cell spreading, migration, and competing taxis. J. Mech. Phys. Solid. *179*, 105390. https://doi.org/10.1016/j.jmps.2023.105390.
68. Zhao, S.Z., Ariff, B., Long, Q., Hughes, A.D., Thom, S.A., Stanton, A.V., and Xu, X.Y. (2002). Inter-individual variations in wall shear stress and mechanical stress distributions at the carotid artery bifurcation of healthy humans. J. Biomech. *35*, 1367–1377.
69. Chen, H.-L., Hsu, F.-T., Kao, Y.-C.J., Liu, H.-S., Huang, W.-Z., Lu, C.-F., Tsai, P.-H., Ali, A.A.A., Lee, G.A., Chen, R.-J., and Chen, C.-Y. (2017). Identification of epidermal growth factor receptor-positive glioblastoma using lipid-encapsulated targeted superparamagnetic iron oxide nanoparticles in vitro. J. Nanobiotechnol. *15*, 86. https://doi.org/10.1186/s12951-017-0313-2.
70. Nimnual, A.S., Taylor, L.J., and Bar-Sagi, D. (2003). Redox-dependent downregulation of Rho by Rac. Nat. Cell Biol. *5*, 236–241. https://doi.org/10.1038/ncb938.
71. Ohta, Y., Hartwig, J.H., and Stossel, T.P. (2006). FilGAP, a Rho- and ROCK-regulated GAP for Rac binds filamin A to control actin remodelling. Nat. Cell Biol. *8*, 803–814. https://doi.org/10.1038/ncb1437.
72. Marée, A.F.M., Grieneisen, V.A., and Edelstein-Keshet, L. (2012). How Cells Integrate Complex Stimuli: The Effect of Feedback from Phosphoinositides and Cell Shape on Cell Polarization and Motility. PLoS Comput. Biol. *8*, e1002402. https://doi.org/10.1371/journal.pcbi.1002402.
73. Dawes, A.T., and Edelstein-Keshet, L. (2007). Phosphoinositides and Rho proteins spatially regulate actin polymerization to initiate and maintain directed movement in a one-dimensional model of a motile cell. Biophys. J. *92*, 744–768. https://doi.org/10.1529/biophysj.106.090514.
74. Holmes, W.R., and Edelstein-Keshet, L. (2016). Analysis of a minimal Rho-GTPase circuit regulating cell shape. Phys. Biol. *13*, 046001. https://doi.org/10.1088/1478-3975/13/4/046001.
75. Sáez, P., and Venturini, C. (2023). Positive, negative and controlled durotaxis. Soft Matter *19*, 2993–3001. https://doi.org/10.1039/D2SM01326F.
76. Kobylkevich, B.M., Sarkar, A., Carlberg, B.R., Huang, L., Ranjit, S., Graham, D.M., and Messerli, M.A. (2018). Reversing the direction of galvanotaxis with controlled increases in boundary layer viscosity. Phys. Biol. *15*, 036005. https://doi.org/10.1088/1478-3975/aaad91.
77. Sun, Y., Reid, B., Zhang, Y., Zhu, K., Ferreira, F., Estrada, A., Sun, Y., Draper, B.W., Yue, H., Copos, C., et al. (2023). Min Zhao, and Alex Mogilner. Electric field–guided collective motility initiation of large epidermal cell groups. Mol. Biol. Cell *34*, ar48. https://doi.org/10.1091/mbc.E22-09-0391.
78. Wilhelm, M., Schlegl, J., Hahne, H., Gholami, A.M., Lieberenz, M., Savitski, M.M., Ziegler, E., Butzmann, L., Gessulat, S., Marx, H., et al. (2014). Mass-spectrometry-based draft of the human proteome. Nature *509*, 582–587. https://doi.org/10.1038/nature13319.
79. Uhlén, M., Fagerberg, L., Hallström, B.M., Lindskog, C., Oksvold, P., Mardinoglu, A., Sivertsson, Å., Kampf, C., Sjöstedt, E., Asplund, A., et al. (2015). Tissue-based map of the human proteome. Science *347*, 1260419. https://doi.org/10.1126/science.1260419.

80. Torres-Sánchez, A., Kerr Winter, M., and Salbreux, G. (2021). Tissue hydraulics: Physics of lumen formation and interaction. Cells Dev. *168*, 203724. https://doi.org/10.1016/j.cdev.2021.203724.

81. Nwogbaga, I., Kim, A.H., and Camley, B.A. (2023). Physical limits on galvanotaxis. Phys. Rev. E *108*, 064411. https://doi.org/10.1103/PhysRevE.108.064411.

82. Nakajima, K.-ichi, Zhu, K., Sun, Y.-H., Hegyi, B., Zeng, Q., Murphy, C.J., Small, J.V., Chen-Izu, Y., Izumiya, Y., Penninger, J.M., and Zhao, M. (2015). KCNJ15/Kir4.2 couples with polyamines to sense weak extracellular electric fields in galvanotaxis. Nat. Commun. *6*, 8532. https://doi.org/10.1038/ncomms9532.

83. Djamgoz, M.B.A., Mycielska, M., Madeja, Z., Fraser, S.P., and Korohoda, W. (2001). Directional movement of rat prostate cancer cells in direct-current electric field: involvement of voltagegated Na+ channel activity. J. Cell Sci. *114*, 2697–2705. https://doi.org/10.1242/jcs.114.14.2697.

84. Cho, M.R., Thatte, H.S., Silvia, M.T., and Golan, D.E. (1999). Transmembrane calcium influx induced by ac electric fields. FASEB J. *13*, 677–683. https://doi.org/10.1096/fasebj.13.6.677.

85. Mycielska, M.E., and Djamgoz, M.B.A. (2004). Cellular mechanisms of direct-current electric field effects: galvanotaxis and metastatic disease. J. Cell Sci. *117*, 1631–1639. https://doi.org/10.1242/jcs.01125.

86. Zhang, Y., Yan, J., Xu, H., Yang, Y., Li, W., Wu, H., and Liu, C. (2018). Extremely low frequency electromagnetic fields promote mesenchymal stem cell migration by increasing intracellular Ca2+ and activating the FAK/Rho GTPases signaling pathways in vitro. Stem Cell Res. Ther. *9*, 143.

87. Li, Y., and Sun, S.X. (2024). Cell migration dynamics explained by the coupling of mechanics with electrochemistry and pH regulation. Phys. Rev. Res. *6*, 023158. https://doi.org/10.1103/PhysRevResearch.6.023158.

88. Ge, Z., Ni, Q., and Sun, S. (2024). The interplay of membrane potential and cytoskeleton directs cell migration. Biophys. J. *123*, 128a. https://doi.org/10.1016/j.bpj.2023.11.88.

89. Levine, S., Levine, M., Sharp, K.A., and Brooks, D.E. (1983). Theory of the electrokinetic behavior of human erythrocytes. Biophys. J. *42*, 127–135. https://doi.org/10.1016/S0006-3495(83)84378-1.

90. Cooper, M.S., and Keller, R.E. (1984). Perpendicular orientation and directional migration of amphibian neural crest cells in dc electrical fields. Proc. Natl. Acad. Sci. USA *81*, 160–164. https://doi.org/10.1073/pnas.81.1.160.

91. Guo, A., Song, B., Reid, B., Gu, Y., Forrester, J.V., Jahoda, C.A.B., and Zhao, M. (2010). Effects of Physiological Electric Fields on Migration of Human Dermal Fibroblasts. J. Invest. Dermatol. *130*, 2320–2327. https://doi.org/10.1038/jid.2010.96.

92. Liu, W.K., Liu, Y., Farrell, D., Zhang, L., Wang, X.S., Fukui, Y., Patankar, N., Zhang, Y., Bajaj, C., Lee, J., et al. (2006). Immersed finite element method and its applications to biological systems. Comput. Methods Appl. Mech. Eng. *195*, 1722–1749. https://doi.org/10.1016/j.cma.2005.05.049.

93. Moure, A., and Gomez, H. (2021). Phase-field modeling of individual and collective cell migration. Arch. Comput. Methods Eng. *28*, 311–344. https://doi.org/10.1007/s11831-019-09377-1.

94. Saw, T.B., Gao, X., Li, M., He, J., Le, A.P., Marsh, S., Lin, K.-hui, Ludwig, A., Prost, J., and Lim, C.T. (2022). Transepithelial potential difference governs epithelial homeostasis by electromechanics. Nat. Phys. *18*, 1122–1128. https://doi.org/10.1038/s41567-022-01657-1.

95. Shim, G., Breinyn, I.B., Martínez-Calvo, A., Rao, S., and Cohen, D.J. (2024). Bioelectric stimulation controls tissue shape and size. Nat. Commun. *15*, 2938. https://doi.org/10.1038/s41467-024-47079-w.

96. Sun, Y., Do, H., Gao, J., Zhao, R., Zhao, M., and Mogilner, A. (2013). Keratocyte fragments and cells utilize competing pathways to move in opposite directions in an electric field. Curr. Biol. *23*, 569–574. https://doi.org/10.1016/j.cub.2013.02.026.

97. Jeon, T.J., Gao, R., Kim, H., Lee, A., Jeon, P., Devreotes, P.N., and Zhao, M. (2019). Cell migration directionality and speed are independently regulated by RasG and Gα in Dictyostelium cells in electrotaxis. Biol. Open *8*, bio042457.

98. Raftopoulou, M., and Hall, A. (2004). Cell migration: Rho GTPases lead the way. Dev. Biol. *265*, 23–32. https://doi.org/10.1016/j.ydbio.2003.06.003.

99. Moon, S.Y., and Zheng, Y. (2003). Rho GTPase-activating proteins in cell regulation. Trends Cell Biol. *13*, 13–22. https://doi.org/10.1016/S0962-8924(02)00004-1.

100. Mitchison, T.J., and Cramer, L.P. (1996). Actin-based cell motility and cell locomotion. Cellule *84*, 371–379.

101. Ridley, A.J. (2001). Rho GTPases and cell migration. J. Cell Sci. *114*, 2713–2722. https://doi.org/10.1242/jcs.114.15.2713.

102. Wedlich-Soldner, R., Altschuler, S., Wu, L., and Li, R. (2003). Spontaneous Cell Polarization Through Actomyosin-Based Delivery of the Cdc42 GTPase. Science *299*, 1231–1235. https://doi.org/10.1126/science.1080944.

103. Chung, C.Y., Lee, S., Briscoe, C., Ellsworth, C., and Firtel, R.A. (2000). Role of Rac in controlling the actin cytoskeleton and chemotaxis in motile cells. Proc. Natl. Acad. Sci. USA *97*, 5225–5230. https://doi.org/10.1073/pnas.97.10.5225.

104. Gardiner, E.M., Pestonjamasp, K.N., Bohl, B.P., Chamberlain, C., Hahn, K.M., and Bokoch, G.M. (2002). Spatial and Temporal Analysis of Rac Activation during Live Neutrophil Chemotaxis. Curr. Biol. *12*, 2029–2034. https://doi.org/10.1016/S0960-9822(02)01334-9.

105. Herzmark, P., Campbell, K., Wang, F., Wong, K., El-Samad, H., Groisman, A., and Bourne, H.R. (2007). Bound attractant at the leading vs. the trailing edge determines chemotactic prowess. Proc. Natl. Acad. Sci. USA *104*, 13349–13354. https://doi.org/10.1073/pnas.0705889104.

106. Weiner, O.D., Servant, G., Welch, M.D., Mitchison, T.J., Sedat, J.W., and Bourne, H.R. (1999). Spatial control of actin polymerization during neutrophil chemotaxis. Nat. Cell Biol. *1*, 75–81. https://doi.org/10.1038/10042.

107. Weiner, O.D., Marganski, W.A., Wu, L.F., Altschuler, S.J., and Kirschner, M.W. (2007). An Actin-Based Wave Generator Organizes Cell Motility. PLoS Biol. *5*, e221. https://doi.org/10.1371/journal.pbio.0050221.

108. Xu, J., Wang, F., Van Keymeulen, A., Herzmark, P., Straight, A., Kelly, K., Takuwa, Y., Sugimoto, N., Mitchison, T., and Bourne, H.R. (2003). Divergent signals and cytoskeletal assemblies regulate self-organizing polarity in neutrophils. Cell *114*, 201–214. https://doi.org/10.1016/S0092-8674(03)00555-5.

109. Srinivasan, S., Wang, F., Glavas, S., Ott, A., Hofmann, F., Aktories, K., Kalman, D., and Bourne, H.R. (2003). Rac and Cdc42 play distinct roles in regulating PI(3,4,5)P3 and polarity during neutrophil chemotaxis. J. Cell Biol. *160*, 375–385. https://doi.org/10.1083/jcb.200208179.

110. Kraynov, V.S., Chamberlain, C., Bokoch, G.M., Schwartz, M.A., Slabaugh, S., and Hahn, K.M. (2000). Localized Rac Activation Dynamics Visualized in Living Cells. Science *290*, 333–337. https://doi.org/10.1126/science.290.5490.333.

111. Nalbant, P., Hodgson, L., Kraynov, V., Toutchkine, A., and Hahn, K.M. (2004). Activation of Endogenous Cdc42 Visualized in Living Cells. Science *305*, 1615–1619. https://doi.org/10.1126/science.1100367.

112. Wong, K., Pertz, O., Hahn, K., and Bourne, H. (2006). Neutrophil polarization: Spatiotemporal dynamics of RhoA activity support a self-organizing mechanism. Proc. Natl. Acad. Sci. USA *103*, 3639–3644. https://doi.org/10.1073/pnas.0600092103.

113. Svitkina, T.M., and Borisy, G.G. (1999). Arp2/3 Complex and Actin Depolymerizing Factor/Cofilin in Dendritic Organization and Treadmilling of Actin Filament Array in Lamellipodia. J. Cell Biol. *145*, 1009–1026. https://doi.org/10.1083/jcb.145.5.1009.

114. Amann, K.J., and Pollard, T.D. (2001). The Arp2/3 complex nucleates actin filament branches from the sides of pre-existing filaments. Nat. Cell Biol. *3*, 306–310. https://doi.org/10.1038/35060104.

115. Prehoda, K.E., Scott, J.A., Mullins, R.D., and Lim, W.A. (2000). Integration of Multiple Signals Through Cooperative Regulation of the N-WASP-Arp2/3 Complex. Science *290*, 801–806. https://doi.org/10.1126/science.290.5492.801.

116. Blanchoin, L., Amann, K.J., Higgs, H.N., Marchand, J.B., Kaiser, D.A., and Pollard, T.D. (2000). Direct observation of dendritic actin filament networks nucleated by Arp2/3 complex and WASP/Scar proteins. Nature *404*, 1007–1011. https://doi.org/10.1038/35010008.

117. Houk, A.R., Jilkine, A., Mejean, C.O., Boltyanskiy, R., Dufresne, E.R., Angenent, S.B., Altschuler, S.J., Wu, L.F., and Weiner, O.D. (2012). Membrane tension maintains cell polarity by confining signals to the leading edge during neutrophil migration. Cell *148*, 175–188. https://doi.org/10.1016/j.cell.2011.10.050.

118. Goehring, N.W., and Grill, S.W. (2013). Cell polarity: Mechanochemical patterning. Trends Cell Biol. *23*, 72–80. https://doi.org/10.1016/j.tcb.2012.10.009.

119. Nobes, C.D., and Hall, A. (1995). Rho, Rac, and Cdc42 GTPases regulate the assembly of multimolecular focal complexes associated with actin stress fibers, lamellipodia, and filopodia. Cell *81*, 53–62. https://doi.org/10.1016/0092-8674(95)90370-4.

120. Itoh, R.E., Kurokawa, K., Ohba, Y., Yoshizaki, H., Mochizuki, N., and Matsuda, M. (2002). Activation of Rac and Cdc42 Video Imaged by Fluorescent Resonance Energy Transfer-Based Single-Molecule Probes in the Membrane of Living Cells. Mol. Cell Biol. *22*, 6582–6591. https://doi.org/10.1128/MCB.22.18.6582-6591.

121. Kimura, K., Ito, M., Amano, M., Chihara, K., Fukata, Y., Nakafuku, M., Yamamori, B., Feng, J., Nakano, T., Okawa, K., et al. (1996). Regulation of Myosin Phosphatase by Rho and Rho-Associated Kinase (Rho-Kinase). Science *273*, 245–248. https://doi.org/10.1126/science.273.5272.245.

122. Bishop, A.L., and Hall, A. (2000). Rho GTPases and their effector proteins. Biochem. J. *348*, 241–255.

123. Zondag, G.C., Evers, E.E., ten Klooster, J.P., Janssen, L., van der Kammen, R.A., and Collard, J.G. (2000). Oncogenic Ras Downregulates Rac Activity, Which Leads to Increased Rho Activity and Epithelial–Mesenchymal Transition. J. Cell Biol. *149*, 775–782. https://doi.org/10.1083/jcb.149.4.775.

124. Giniger, E. (2002). How do Rho family GTPases direct axon growth and guidance? A proposal relating signaling pathways to growth cone mechanics. Differentiation *70*, 385–396. https://doi.org/10.1046/j.1432-0436.2002.700801.x.

125. Tsuji, T., Ishizaki, T., Okamoto, M., Higashida, C., Kimura, K., Furuyashiki, T., Arakawa, Y., Birge, R.B., Nakamoto, T., Hirai, H., and Narumiya, S. (2002). ROCK and mDia1 antagonize in Rho-dependent Rac activation in Swiss 3T3 fibroblasts. J. Cell Biol. *157*, 819–830. https://doi.org/10.1083/jcb.200112107.

126. Worthylake, R.A., and Burridge, K. (2003). RhoA and ROCK Promote Migration by Limiting Membrane Protrusions. J. Biol. Chem. *278*, 13578–13584. https://doi.org/10.1074/jbc.M211584200.

127. Sander, E.E., van Delft, S., ten Klooster, J.P., Reid, T., van der Kammen, R.A., Michiels, F., and Collard, J.G. (1998). Matrix-dependent Tiam1/Rac Signaling in Epithelial Cells Promotes Either Cell–Cell Adhesion or Cell Migration and Is Regulated by Phosphatidylinositol 3-Kinase. J. Cell Biol. *143*, 1385–1398. https://doi.org/10.1083/jcb.143.5.1385.

128. Zheng, Y., Bagrodia, S., and Cerione, R.A. (1994). Activation of phosphoinositide 3-kinase activity by Cdc42Hs binding to p85. J. Biol. Chem. *269*, 18727–18730. https://doi.org/10.1016/S0021-9258(17)32226-3.

129. Merlot, S., and Firtel, R.A. (2003). Leading the way: directional sensing through phosphatidylinositol 3-kinase and other signaling pathways. J. Cell Sci. *116*, 3471–3478. https://doi.org/10.1242/jcs.00703.

130. Weiner, O.D., Neilsen, P.O., Prestwich, G.D., Kirschner, M.W., Cantley, L.C., and Bourne, H.R. (2002). A PtdInsP3- and Rho GTPase-mediated positive feedback loop regulates neutrophil polarity. Nat. Cell Biol. *4*, 509–513. https://doi.org/10.1038/ncb811.

131. Welch, H.C.E., Coadwell, W.J., Stephens, L.R., and Hawkins, P.T. (2003). Phosphoinositide 3-kinase-dependent activation of Rac. FEBS Lett. *546*, 93–97. https://doi.org/10.1016/S0014-5793(03)00454-X.

132. Tolias, K.F., Hartwig, J.H., Ishihara, H., Shibasaki, Y., Cantley, L.C., and Carpenter, C.L. (2000). Type Iα phosphatidylinositol-4-phosphate 5-kinase mediates Rac-dependent actin assembly. Curr. Biol. *10*, 153–156. https://doi.org/10.1016/S0960-9822(00)00315-8. https://linkinghub.elsevier.com/retrieve/pii/S0960982200003158.

133. Czech, M.P. (2000). PIP2 and PIP3: Complex Roles at the Cell Surface. Cell *100*, 603–606. https://doi.org/10.1016/S0092-8674(00)80696-0.

134. Rickert, P., Weiner, O.D., Wang, F., Bourne, H.R., and Servant, G. (2000). Leukocytes navigate by compass: roles of PI3K and its lipid products. Trends Cell Biol. *10*, 466–473.

135. Papayannopoulos, V., Co, C., Prehoda, K.E., Snapper, S., Taunton, J., and Lim, W.A. (2005). A Polybasic Motif Allows N-WASP to Act as a Sensor of PIP2 Density. Mol. Cell *17*, 181–191. https://doi.org/10.1016/j.molcel.2004.11.054.

136. Ann, M.R., Foubister, L.E., and McCaig, C.D. (2006). Growth cone steering by a physiological electric _eld requires dynamic microtubules, micro_laments and Rac-mediated filopodial asymmetry. J. Cell Sci. *119*, 1736–1745. https://doi.org/10.1242/jcs.02897.

137. Yeung, T., Gilbert, G.E., Shi, J., Silvius, J., Kapus, A., and Grinstein, S. (2008). Membrane phosphatidylserine regulates surface charge and protein localization. Science *319*, 210–213. https://doi.org/10.1126/science.1152066.

138. Rohatgi, R., Ma, L., Miki, H., Lopez, M., Kirchhausen, T., Takenawa, T., and Kirschner, M.W. (1999). The Interaction between N-WASP and the Arp2/3 Complex Links Cdc42-Dependent Signals to Actin Assembly. Cell *97*, 221–231. https://doi.org/10.1016/S0092-8674(00)80732-1.

139. Higgs, H.N., and Pollard, T.D. (2000). Activation by Cdc42 and Pip2 of Wiskott-Aldrich Syndrome Protein (Wasp) Stimulates Actin Nucleation by Arp2/3 Complex. J. Cell Biol. *150*, 1311–1320. https://doi.org/10.1083/jcb.150.6.1311.

140. Rohatgi, R., Nollau, P., Ho, H.Y., Kirschner, M.W., and Mayer, B.J. (2001). Nck and Phosphatidylinositol 4,5-Bisphosphate Synergistically Activate Actin Polymerization through the N-WASP-Arp2/3 Pathway. J. Biol. Chem. *276*, 26448–26452. https://doi.org/10.1074/jbc.M103856200.

141. Wang, F., Herzmark, P., Weiner, O.D., Srinivasan, S., Servant, G., and Bourne, H.R. (2002). Lipid products of PI(3)Ks maintain persistent cell polarity and directed motility in neutrophils. Nat. Cell Biol. *4*, 513–518. https://www.nature.com/articles/ncb810.

142. Hawkins, P.T., Eguinoa, A., Qiu, R.G., Stokoe, D., Cooke, F.T., Walters, R., Wennström, S., Claesson-Welsh, L., Evans, T., Symons, M., and Stephens, L. (1995). PDGF stimulates an increase in GTP–Rac via activation of phosphoinosi tide 3-kinase. Curr. Biol. *5*, 393–403. https://doi.org/10.1016/S0960-9822(95)00080-7.

143. Song, L., Huang, N.F., and Hsu, S. (2005). Mechanotransduction in endothelial cell migration. J. Cell. Biochem. *96*, 1110–1126. https://doi.org/10.1002/jcb.20614.

144. Funamoto, S., Meili, R., Lee, S., Parry, L., and Firtel, R.A. (2002). Spatial and Temporal Regulation of 3-Phosphoinositides by PI 3-Kinase and PTEN Mediates Chemotaxis. Cell *109*, 611–623. https://doi.org/10.1016/S0092-8674(02)00755-9.

145. Iijima, M., and Devreotes, P. (2002). Tumor Suppressor PTEN Mediates Sensing of Chemoattractant Gradients. Cell *109*, 599–610. https://doi.org/10.1016/S0092-8674(02)00745-6.

146. Huang, Y.E., Iijima, M., Parent, C.A., Funamoto, S., Firtel, R.A., and Devreotes, P. (2003). Receptor-mediated Regulation of PI3Ks Con_nes

PI(3,4,5)P 3 to the Leading Edge of Chemotaxing Cells. Mol. Biol. Cell *14*, 1913–1922. https://doi.org/10.1091/mbc.e02-10-0703.

147. Jiménez, C., Portela, R.A., Mellado, M., Rodríguez-Frade, J.M., Collard, J., Serrano, A., Martínez-A, C., Avila, J., and Carrera, A.C. (2000). Role of the Pi3k Regulatory Subunit in the Control of Actin Organization and Cell Migration. J. Cell Biol. *151*, 249–262. https://doi.org/10.1083/jcb.151.2.249.

148. Franca-Koh, J., Kamimura, Y., and Devreotes, P.N. (2007). Leading-edge research: PtdIns(3,4,5)P3 and directed migration. Nat. Cell Biol. *9*, 15–17. https://doi.org/10.1038/ncb0107-15.

149. Ferguson, G.J., Milne, L., Kulkarni, S., Sasaki, T., Walker, S., Andrews, S., Crabbe, T., Finan, P., Jones, G., Jackson, S., et al. (2007). PI(3)K has an important context-dependent role in neutrophil chemokinesis. Nat. Cell Biol. *9*, 86–91. https://doi.org/10.1038/ncb1517.

150. Nishio, M., Watanabe, K.i., Sasaki, J., Taya, C., Takasuga, S., Iizuka, R., Balla, T., Yamazaki, M., Watanabe, H., Itoh, R., et al. (2007). Control of cell polarity and motility by the PtdIns(3,4,5)P3 phosphatase SHIP1. Nat. Cell Biol. *9*, 36–44. https://doi.org/10.1038/ncb1515.

151. Kutscher, B., Devreotes, P., and Pablo, A. (2004). Iglesias. Local Excitation, Global Inhibition Mechanism for Gradient Sensing: An Interactive Applet. Sci. STKE *2004*, pl3. https://doi.org/10.1126/stke.2192004pl3.

152. Donea, J., and Huerta, A. (2003). Finite Element Methods for Ow Problems (Wiley), pp. 1–358. https://doi.org/10.1002/0470013826.

153. Szklarczyk, D., Kirsch, R., Koutrouli, M., Nastou, K., Mehryary, F., Hachilif, R., Gable, A.L., Fang, T., Doncheva, N.T., Pyysalo, S., et al. (2023). The STRING database in 2023: protein–protein association networks and functional enrichment analyses for any sequenced genome of interest. Nucleic Acids Res. *51*, D638–D646. https://doi.org/10.1093/nar/gkac1000.

154. UniProt Consortium (2023). UniProt: the Universal Protein Knowledgebase in 2023. Nucleic Acids Res. *51*, D523–D531. https://doi.org/10.1093/nar/gkac1052.

155. Bradford, Y.M., Van Slyke, C.E., Ruzicka, L., Singer, A., Eagle, A., Fashena, D., Howe, D.G., Frazer, K., Martin, R., Paddock, H., et al. (2022). Zebra_sh information network, the knowledgebase for Danio rerio research. Gene *220*, iyac016. https://doi.org/10.1093/genetics/iyac016.

STAR★METHODS

KEY RESOURCES TABLE

REAGENT or RESOURCE	SOURCE	IDENTIFIER
Deposited data		
List of the zebrafish proteome with physical properties	Sarkar et al.[40]	https://doi.org/10.1016/j.jtbi.2019.06.015
Dataset1: Zebrafish proteome analysis with physical properties and electromigration velocities.	This Paper	N/A
Dataset2: Zebrafish proteome analysis with identified signaling pathways.	This Paper	N/A
Dataset3: Zebrafish proteome analysis with physical properties and electromigration velocities when the EDL forms around CMPs.	This Paper	N/A
Dataset4: Zebrafish proteome analysis with identified signaling pathways when the EDL forms around CMPs	This Paper	N/A
Software and algorithms		
Electrotaxis code	This Paper	https://es.mathworks.com/matlabcentral/fileexchange/166511-electrotaxis_1d
MATLAB 2024a	The MathWorks, Inc.	https://www.mathworks.com/products/matlab.html
Seaborn (v 0.11.2)	Michael Waskom	https://seaborn.pydata.org/archive/0.11/index.html

METHOD DETAILS

To model the cascade of events toward electrotaxis, we consider a one-dimensional computational model. The cell domain, Ω, is a continuum segment with moving coordinates $x(t) \in [l_a(t), l_c(t)]$, where $l_a(t)$ and $l_c(t)$ represents the anodal and cathodal facing boundaries of the cell and, therefore, the length of the cell is determined as $L(t) = |l_a(t) - l_c(t)|$. The boundary velocities will be given by $\dot{l}_a(t)$ and $\dot{l}_c(t)$, which are described next. The moving of both cell ends will depend on the velocity of the contractile actomyosin network and the velocity of actin polymerization at the cathodal and anodal fronts, which will eventually dictate the migration direction and velocity of the cell.

To model the cascade of events toward electrotaxis, we look first into the first cell sensors. If an EF can only be sensed outside the cell, then CMPs should be directly, uniquely, and firstly implicated in these opposing electrotactic responses. Therefore, we model the electro-motility of CMPs,[38,40,61] which are then responsible for the downstream polarization of intracellular signals. To reproduce the signaling layer of the process we based on previous models from literature.[62–64,72–74] Finally, we use our previous active gel models of cell migration to computationally analyze the coupling of GTPases with migration forces of the cell under the effect of the EF.[67]

Electromotility of charged membrane components

CMPs experience two opposing forces. When cells are immersed in electrolytes, the negative charge of the cell membrane makes positive ions accumulate nearby and develop a well-differentiated region known as the Electrical Double Layer (EDL), whose thickness is of the order of the ionic radius. When an EF is imposed on a cell, the EDL is also exposed to the field and drags the fluid around it. This creates an electrically generated fluid flow known as electro-osmotic flow (EOF). Embedded on the cell surface, CMPs are dragged by the EOF and, consequently can migrate along the cell membrane. Besides, these charged particles move due to electrostatic attraction and also experience a local EOF around that drag them. The effect of these two phenomena is referred to as electrophoresis.

The drag forces from the EOF and electrophoretic attraction redistribute CMPs asymmetrically along the cell membrane,[38,40,61] generating a cathode-anode axis of polarity in cells. To measure the rate and intensity of this redistribution due to the electrophoretic

and electro-osmotic mobilities of the CMPs, we use the 'tethered sphere model' to simplify the geometry of CMP, which results in the total electro-motility velocity,

$$v_e = \frac{\epsilon_r \epsilon_0 E(\zeta_1 - \zeta_2)}{\eta_m}, \quad \text{(Equation 1)}$$

where ϵ_r is the dielectric constant of the medium, ϵ_0 is the permittivity of free space, E is the applied Electric field strength, η_m represents the viscosity of the cell membrane and ζ_1 and ζ_2 are the ζ-potential of the CMPs and the cell surface, respectively. This v_e represents the classical expression derived in,[61] which we follow in most of our results. However, to reproduce the results in Figure 3, where we focus on the zebrafish keratocyte proteome,[40] we cannot calculate the electrophoresis motility as a function of the zeta potential, because we do n't directly know it. In this case, we followed two approaches (see Methods S1 for details): First, we use the Einstein relation to calculate the electrophoretic mobility assuming that the EDL is not formed. Second, we compute the zeta potential as a function of the net external charge and apparent radius of each protein. To describe the distribution of positive and negative CMPs, $\rho_\pm$, in space and time, we use a convection-diffusion equation:

$$\partial_t \rho_\pm + \partial_x (v_e \pm \rho_\pm - D_M \partial_x \rho_\pm) = 0, \quad \text{(Equation 2)}$$

where D_M is the diffusion coefficient for CMPs. We assume zero Neumann boundary conditions at both ends for $\rho_\pm$ to consider that no CMP can enter or leave the cell membrane. We also consider a normalized homogeneous initial condition $\rho_\pm(x,0) = 1$.

Signaling pathways and mathematical model

Specifically, Cdc42, Rac1, and RhoA, members of the family of Rho-GTPases and highly conserved in various eukaryotic cells, are directly involved in regulating the motility forces of the cell such as actin polymerization,[53] myosin contractility[26,96,97] and cell adhesion.[42] These members of the Rho family proteins alternate between an active GTP-bound state on the membrane and an inactive GDP-bound state on the membrane or in the cytosol. They activate in response to Guanine nucleotide exchange factors (GEFs) by promoting the replacement of GDP with GTP, while GTPase-activating proteins (GAPs) accelerate GTP hydrolysis, leading to protein inactivation.[98,99] When a ligand activates polarized GPCRs and RTKs, it also induces a polarized expression of GEFs, which propagates downstream to generate a polarization of Rho-GTPases. The active forms of Rho GTPases regulate the activity of numerous proteins involved in cytoskeletal processes, influencing the polymerization and depolymerization of the actin cytoskeleton.[100–103] Cdc42 and Rac are highly concentrated at the leading edge[104–107] and Rho is predominantly localized at the rear.[108–112] Rac recruits downstream effectors such as Arp2/3 and the Scar/WAVE complex. Arp2/3 is activated near the membrane by WASp or N-WASp and facilitates side-branching, nucleation of new barbed ends[113–116] and polymerization against the cell membrane.[53] As a result, actin-driven membrane protrusions form at regions of high Rac activity, leading to an increase in cell surface area and inducing a global rise in membrane tension.[117,118] Similar to Rac, Cdc42 interacts with membrane-associated proteins like WASp or N-WASp, promoting the activation of Arp2/3. Cdc42 can also activate Rac.[119] Active Rac forms a gradient with the highest concentration at the leading edge of migrating Swiss 3T3 fibroblasts.[110] Similar experiments have shown high levels of active Cdc42 at cell edges undergoing remodeling.[111] Gradients of active Cdc42 and Rac, with the highest concentration at the leading edge, have been detected in motile HT1080 cells.[120] Rho, on the other hand, promotes myosin light chain phosphorylation through Rho kinase (ROCK).[101,121,122] Importantly, it is believed that the distribution of active Rho is inverse to that of Cdc42 and Rac in motile cells[98,123] thanks to mutual inhibitory feedback loops between Rac and RhoA.[70,71,124] ROCK can suppress Rac activity by targeting specific Rac-specific GEFs and GAPs.[71,125,126] Cdc42 has been also shown to have both positive and negative regulatory effects on Rho activation while Rho, in turn, acts as a local antagonist to Cdc42.[127] In neutrophils, mutual exclusion between Cdc42 and Rho has been also observed.[124]

The polarized GPCRs and RTKs can also induce a polarized expression of membrane lipids, PI(4)P, PI(4,5) P_2, and PI(3,4,5) P_3 (PIP, PIP2, and PIP3), Phosphoinositide 3-kinase (PI3K) and phosphoinositide-4-phosphate 5-kinases (PI5Ks), which are involved in the directed cell migration during electrotaxis.[23,45] Active Cdc42 and Rac activate PI3K[109,128,129] which generates PIP3 from PIP2, which becomes upregulated at the cell location closest to a stimulating signal.[130,131] Rac has been also shown to interact with PI5K, which converts PIP to PIP2, to enhance their activity.[132,133] In a positive close loop, Rac activation is dependent on PI3K and its inhibition blocks Rac activation.[127,134] On the other hand, PTEN, which converts PIP3 back to PIP2, shifts to the opposite end. Indeed, PIP2 is central to cell migration because it activates actin polymerization[115,135] and Cdc42 and recruits Rac[136] which, in turn, controls cell polarity[137] and activate the PI3K-Akt pathway.[16] Moreover, PIP2 inhibits the association of capping protein with the barbed ends of actin filaments[101] and it is required to activate WASp and N-WASp, which subsequently activate Arp2/3.[138–140] On the other hand, PIP3 is necessary for the activation of Cdc42 and Rac.[109,130,141,142] Additionally, Rho activates Rho kinase, which activates PTEN, influencing its spatial exclusion from regions with high PI3K and Cdc42 activity.[143] When a cell is exposed to a chemoattractant gradient, PTEN is released from the membrane at the cell's front, allowing PI3K to associate with the membrane. PTEN remains bound to the sides and back of the stimulated cell. This spatial redistribution of PI3K and PTEN leads to elevated levels of PIP3 at the leading edge.[144–146] Inhibiting PI3K has been shown to affect cell polarity and motility in some cases but not in others, leading to uncertainties regarding the roles of phosphoinositides in chemotaxis.[134,141,147] It has been also shown that mammalian neutrophils and Dictyostelium discoideum cells polarize with no PI3K activity.[148–150] In terms of phosphoinositides, high concentrations of PIP provide more substrate for the formation of PIP3, through increased PIP2 formation. Assuming that adaptation occurs

downstream of G-protein activation, it implies that the G-protein and its effectors, including PI3K, remain elevated as long as the ligand is present.

Polarization of signaling cues by the LEGI model

The LEGI model represents one of the simplest still more comprehensive models to account for these mentioned interactions. It proposes PI3K and PTEN as activator (A) and inhibitor (I), respectively, of a response element (R), which represents small GTPases. Specifically, we assume R to be associated with Rac and Cdc42, which activates the cell front through actin filament polymerization. Because Rac1 and Cdc42 are mutually exclusive to RhoA,[70,71] we assume the density of Rho A, ρ, to be equal but in the opposite direction to R. The LEGI model accounts for all the main signaling aspects summarized in the introduction while simplifying many of the interactions and it is described by the following system of PDEs[151]:

$$\partial_t A = k_A \rho_{\pm} - k_{-A} A, \quad \text{(Equation 3)}$$

$$\partial_t I = D_i \partial_x^2 I + k_I \rho_{\pm} - k_{-I} I \quad \text{(Equation 4)}$$

$$\partial_t R = k_R A - k_{-R} I R. \quad \text{(Equation 5)}$$

The on/off rates for each variable are denoted by k_i and k_{-i}, respectively. The diffusion parameter for the inhibition process is denoted by D_i. Following the hypothesis that redistribution of CMPs is responsible for electrotaxis, we take the CMP density, $\rho_{\pm}$, described previously in Equation 2, as the stimuli for cell polarization. The fast-acting local activator and the slow global inhibitor are activated in direct proportion to the temporal stimuli.

Polarization of signaling cues by a GTPases model

We incorporated a second, more complex model that takes into account explicitly most of the interactions described above (see[72] for further details). All model parameters and their values are summarized in the Table S1. In summary, the active forms of Rac, Cdc42, and Rho are, respectively:

$$\frac{\partial R}{\partial t} = (I_R + \alpha C)\left((1 - f_2) + f_2 \frac{P_3}{P_{3b}}\right) \frac{R_i}{R_{tot}} - d_R R + D_m \partial_x^2 R, \quad \text{(Equation 6)}$$

$$\frac{\partial C}{\partial t} = \left(\frac{I_C}{\left(1+\left(\frac{\rho}{a_1}\right)^n\right)}\right)\left((1 - f_1) + f_1 \frac{P_3}{P_{3b}}\right) \frac{C_i}{C_{tot}} - d_C C + D_m \partial_x^2 C \quad \text{(Equation 7)}$$

$$\frac{\partial \rho}{\partial t} = \left(\frac{(I_\rho + \beta R)}{\left(1+\left(\frac{C}{a_2}\right)^n\right)}\right) \frac{\rho_i}{\rho_{tot}} - d_\rho \rho + D_m \partial_x^2 \rho, \quad \text{(Equation 8)}$$

respectively. The C_{tot}, R_{tot}, ρ_{tot} are the total concentrations of the Cdc42, Rac and Rho. I_c, I_R and I_ρ are activation rates, which we describe below. The values a_1 and a_2 are the Rho and Cdc42 concentrations that elicit a half-maximal drop of Cdc42 and Rho activation, respectively. The value α determines the rate of Cdc42-enhanced activation of Rac, and β determines the rate of Rac-enhanced Rho activation. P_{3b} is the baseline concentration of PIP3 found in a resting cell. d_R, d_C, and d_ρ are the decay rates of activated Rac1, Cdc42 and Rho, respectively. D_m is the diffusion constant of the active form. f_1 and f_2 are feedback from PIP_3 to Cdc42 and Rac, respectively, which we assume differs from the original model,[72] and they are bounded such that $0 \leq f_1, f_2, \leq 1$. This allows us to analyze different feedback strengths from PIP3 to Rac1 and Cdc42.

R_i, C_i, ρ_i are the concentrations of the respective inactive forms, which satisfy the equations:

$$\frac{\partial R_i}{\partial t} = -(I_R + \alpha C)\left((1 - f_2) + f_2 \frac{P_3}{P_{3b}}\right) \frac{R_i}{R_{tot}} + d_R R + D_{mc} \partial_x^2 R, \quad \text{(Equation 9)}$$

$$\frac{\partial C_i}{\partial t} = -\left(\frac{I_C}{\left(1+\left(\frac{\rho}{a_1}\right)^n\right)}\right)\left((1 - f_1) + f_1 \frac{P_3}{P_{3b}}\right) \frac{C_i}{C_{tot}} + d_C C + D_{mc} \partial_x^2 C \quad \text{(Equation 10)}$$

$$\frac{\partial \rho_i}{\partial t} = -\frac{(I_\rho+\beta R)}{\left(1+\left(\frac{C}{a_2}\right)^n\right)}\frac{\rho_i}{\rho_{tot}} + d_\rho \rho + D_{mc}\partial_x^2\rho. \quad \text{(Equation 11)}$$

D_{mc} is the diffusion coefficient of inactive Rho-proteins, which averages the respective diffusion rates of inactive GTPase forms by the time spent on the membrane versus the cytosol and diffuses much faster than the active forms ($D_m \ll D_{mc}$).

We also modified this previous model to include the stimuli from CMPs. This allows us to introduce the stimuli from the polarization of CMPs. To do so, we assume the activation rates I_c, I_R and k_{pi3k} to be dependent on the magnitude of CMPs, which we assume to act as activators. We assume that

$$I_R = (\overline{\rho_\pm} + S_R(\rho_\pm - \overline{\rho_\pm}))I_R^*, \quad \text{(Equation 12)}$$

$$I_C = (\overline{\rho_\pm} + S_C(\rho_\pm - \overline{\rho_\pm}))I_C^*, \quad \text{(Equation 13)}$$

$$k_{pi3k} = (\overline{\rho_\pm} + S_P(\rho_\pm - \overline{\rho_\pm}))k_{pi3k}^*, \quad \text{(Equation 14)}$$

where S_R, S_C, and S_P indicate activation strength factors, where a factor equal to zero indicates that the polarization of the CMPs is not transmitted downstream and, then, the activation will depend on baseline constant conversion rates I_R^*, I_C^* and k_{pi3k}^*, as defined in the base model.[72] $\overline{\rho_\pm}$ is the average value of the density of CMPs $(\rho_\pm)$. We do not include an explicit strength factor for Rho as Rac and Rho are mutually exclusive.

Interactions between GTPases and PIPs are included in coupling terms between these sets of PDEs. The interaction between phosphoinositides, PIP (P_1), PIP2 (P_2), and PIP3 (P_3), and between phosphoinositide kinases, are also modeled by a set of similar PDEs with reaction kinetics as

$$\partial_t P_1 - D_p\partial_x^2 P_1 = I_{P1} - \delta_{P1}P_1 + k_{21}P_2 - f_{PI5K}P_1 \quad \text{(Equation 15)}$$

$$\partial_t P_2 - D_p\partial_x^2 P_2 = -k_{21}P_2 + f_{PI5K}P_1 - f_{PI3K}P_2 + f_{PTEN}P_3 \quad \text{(Equation 16)}$$

$$\partial_t P_3 - D_p\partial_x^2 P_3 = f_{PI3K}P_2 - f_{PTEN}P_3 \quad \text{(Equation 17)}$$

where it is assumed that the conversion to PIP occurs at a constant rate, I_{P1}, and that all PIs diffuse in the membrane at a uniform rate D_p. δ_{P1} is the PIP_1 decay rate and k_{21} is the PIP_2 to PIP_1 conversion rate. The model also describes the fact that Rac enhances the conversion of PIP to PIP2 (via PI5K), of PIP2 to PIP3 (via PI3K), and that Rho enhances the conversion of PIP3 to PIP2 via PTEN. The feedbacks are incorporated through the functions

$$f_{PI5K} = \frac{k_{pi5k}}{2}\left(1+\frac{R}{R_b}\right), \quad \text{(Equation 18)}$$

$$f_{PI3K} = \frac{k_{pi3k}}{2}\left(1+\frac{R}{R_b}\right), \quad \text{(Equation 19)}$$

$$f_{PTEN} = \frac{k_{pten}}{2}\left(1+\frac{\rho}{\rho_b}\right), \quad \text{(Equation 20)}$$

where k_{PI3K} is the PIP_2 to PIP_3 baseline conversion rate, k_{PI5K} is the PIP_1 to PIP_2 baseline conversion rate and k_{PTEN} is the PIP_3 to PIP_2 baseline conversion rate. Whenever we modify k_{pi3k} we also simultaneously adjust k_{pten},as they are the forward and backward rates of the same reaction. This is done with ρ_- and the same strength factor S_P. R_b, C_b and ρ_b are typical levels of active Rac, Cdc42 and Rho respectively.

Mechanical model of the actomyosin network

We consider an active gel model to reproduce the mechanics of actomyosin network[66,67] as

$$\partial_x \sigma = \eta v^F \quad \text{in} \quad \Omega \quad \text{(Equation 21)}$$

where we neglect inertial terms and assume a constitutive relation for the internal stresses, $\sigma = -2\mu\partial_x v^F + \zeta\rho\rho^F\rho^M$, that accounts for the viscosity of the actin cortex and the actomyosin contractibility, respectively. ρ^F and ρ^M are associated with the F-actin and bound myosin motors, as described in the following sections. v is the velocity of the actin network or retrograde flow in the lab frame, μ is its shear viscosity and ζ is the active contraction exerted by the contractile myosin motors that we multiplied by ρ to increase contractibility in the region with a high concentration of RhoA. The term on the r.h.s. represent the friction between the moving cell and the

external space, which we assume to be proportional to the cortex velocity with constant friction η.[67,75] We impose zero Neumann boundary conditions on both ends of the cell.

Kinetics of the cell fronts

The polymerization velocity is regulated biochemically by Rac1 and Cdc42, which regulate Arp2/3 and filament assembly,[53] and physically by the membrane tension, $\tau(L(t))$, that opposes it. We assume the cell membrane tension to be determined by a linear relation $\tau = -k(L(t) - L_0)$, where k is the stiffness of the cell membrane and L_0 is the initial cell length.

Here, we adopt a well established model[65] where the tension-free polymerization velocity $v_0^p = k_{on}\delta R$ is reduced as a function of the membrane tension as

$$v^p = v_0^p\left[1 - \left(\tau(L(t)/\tau_{stall})\right]^{\gamma}. \quad \text{(Equation 22)}$$

k_{on} is the rate of actin assembly at the front, τ_{stall} is the tension required to stall the actin network, γ is a model parameter that controls the velocity decay and δ is the size of one single monomer at the tip of the filament. The function of v_0^p on R makes actin protrusions enhanced at the cell front with high levels of Rac1 and Cdc42 and inhibited at the rear.

If we know the retrograde flow velocity, v, and the polymerization velocity, v^p, we can compute the velocity of the cell front and rear as the result of the inward retrograde flow and the outward polymerization velocity of actin against the plasma membrane. Therefore, the velocity of both ends of the cell is $\dot{l_f}(t) = v_f + v_f^p$ and $\dot{l_b}(t) = v_b + v_b^p$, respectively. Finally, we compute the migration velocity as

$$v = [\dot{l_f}(t) + \dot{l_b}(t)]/2. \quad \text{(Equation 23)}$$

Transport of the actomyosin network

To model the actomyosin network density, we assume for simplicity a filament (F-actin), $\rho^F(x,t)$, and a monomeric (G-actin), $\rho^G(x,t)$, form (see details in[67] and references therein). We use a coupled convection-diffusion model to describe the transport and turnover of actin in the cell:

$$\partial_t\rho^F + \partial_x\left(w\rho^F - D^F\,\partial_x\rho^F\right) = k_p\rho^G - k_d\rho^F \quad \text{(Equation 24)}$$

$$\partial_t\rho^G - \partial_x\left(D^G\,\partial_x\rho^G\right) = k_d\rho^F - k_p\rho^G, \quad \text{(Equation 25)}$$

where D^F and D^G are the diffusion parameters for the F-actin and the G-actin, respectively. k_d and k_p are the depolymerization and polymerization rates. We assume that the diffusivity of the G-actin dominates and the convective term can be neglected. We define the retrograde flow in the cell frame as $w = v^F - v$. We impose zero flux boundary conditions at both cell ends to describe that no actin form can enter or leave the cell membrane.

We also consider a two-species model of myosin motors, a form bound to the F-actin network, ρ^M, and an unbound form, ρ^m. The redistribution of ρ^M and ρ^m is again modeled through a convection-diffusion equation as

$$\partial_t\rho^M + \partial_x\left(w\rho^M - D^M\,\partial_x\rho^M\right) = k_b^M\rho^m - k_u^m\rho^M \quad \text{(Equation 26)}$$

$$\partial_t\rho^m - D^m\,\partial_x^2\rho^m = k_u^m\rho^M - k_b^M\rho^m, \quad \text{(Equation 27)}$$

where D^M and D^m are the diffusion parameters for the bound and unbound forms of myosin, respectively. k_b^M and k_u^m are the binding and unbinding rates of myosin to the F-actin. Again, we assume that the diffusivity of the unbound myosin dominates the convective term. We also assume zero-flux boundary conditions at both cell ends, to describe that no myosin form can enter or leave the cell membrane.

Numerical solution of the problem and model parameters

We solve computationally the coupled system of Equations 2, 3, 4, 5, 6, 7, 8, 9, 10, 11, 12, 13, 14, 15, 16, 17, 18, 19, 20, 21, 24, 25, 26, and 27 in a staggered way. We use the Finite Element Method (FEM) to discretize the system of equations in space and an implicit second-order Crank-Nicholson method to discretize the parabolic equations in time.[152] The non-linear system of equations (Equation 5) is solved iteratively using the Newton-Raphson method.

The FE solution of the parabolic equations will oscillate if $Pe > 1$ (i.e., if the problem becomes convective dominant). As the convective velocity, w, is not known *a priori*, we cannot guarantee that $Pe < 1$. Therefore, we include a Stream-Upwind Petrov Galerkin (SUPG) stabilization term to keep the number of elements of our domain constant and overcome numerical oscillations in our solution.[67,152]

Unless specified otherwise, all model parameters used in the simulations are summarized in Table S1.

Proteomic analysis

To analyze the proteins involved in electrotaxis, we took a previous proteomic analysis of zebrafish keratocytes (see[40] for details). In short, the zebrafish proteome was downloaded from the NCBI website. The proteins were organized into transmembrane, integral, and GPI-anchored proteins, and physical properties were added to the dataset. Then, we complete the dataset with the computed electromigration velocity and direction. For transmembrane proteins, we separated the proteins accumulating toward the anode and the cathode, where we screened them through STRING Database User Survey[153] to obtain those proteins more prevalent in the plasma membrane. For those selected proteins, we check their biological function in the UniProt Consortium[154] and the Zebrafish Information Network (ZFIN)[155] database to find those proteins directly related to signaling in cell migration, either with positive or negative effects.

QUANTIFICATION AND STATISTICAL ANALYSIS

For Figures 3, S4–S6, N represents the number of proteins analyzed. This was provided in the zebrafish proteome dataset. Scatterplots in Figures 3C, 3D, S4A, and S4B were generated using the scatter function in MATLAB R2024a. Probability Density Functions (PDFs) in Figures 3E, 3F, S4C, and S4D were estimated and plotted with the kdeplot (kernel density estimation) function in the Python library Seaborn (v 0.11.2). Boxplots in Figures S5A and S5B were generated using the boxplot function in Seaborn (v 0.11.2), with the median velocity reported as the central value. Finally, the table in Figure S6 summarizes the analyses performed on Data S1–S4, where the mean velocity and standard deviation were calculated in Microsoft Excel, and the median velocity values were taken directly from the boxplots generated in Seaborn (v 0.11.2). In all cases, the mean is the average velocity of the distribution, and the standard deviation provides the measure of spread. The median is the 'middlemost' value in the velocity distribution, meaning half the observations lie below it and half lie above it.